Ultrastructure of the plant cell wall - link to biomechanics -

(Laboratory of Biomass Morphogenesis and Information)
RISH, Kyoto University

Junji Sugiyama

Wood in forest trees undergoes internal stresses during the whole life. Such stress is a potential of the material to strain or even to crack when processed. However, the living tree takes advantages of the stress: tensile longitudinal stress protects sapwood against excessive outer forces such as wind inducing compressive bending stress.

The tension wood is one of the extreme responses of hardwood trees to keep the stem upright or to adjust branches at certain angle to the stem. At the microscopic level, such reaction is found by the formation of G fibers, where the cellulose microfibrils are aligned nearly parallel to the fiber axes. This appears in the upper part of the branch or inclined stem and exert high tensile strength.

At the tree level, the apparition of a tensile stress in the newly formed wood layers is related to the conjunction of two facts: during its formation, the wood have a spontaneous tendency to shrink longitudinally; but this tendency is impeded because the new wood is strongly glued to the internal older wood, so that a tensile longitudinal stress results. The magnitude of the maturation stress can be estimated at the surface of living trees, by mechanically dissociating a portion of wood from the rest of the tree, and recording the generated strain. The order of magnitude of the measured longitudinal strains is around to ca. 300 microstrains (μm/m) in normal wood and can be up to ca. 3000 microstrains in tension wood.

The present study focuses on the role of cellulose crystal in relation to such growth stress in tension wood. The branches from poplar tension wood were introduced to the beam line BL40XU, and the WAXS patterns were collected by the exposure less than second. After taking the first diagram, the sample was trimmed by sawing to release the longitudinal stress. Then, the second diagram was taken without delay. These lines of experiments demonstrate that, before the stress release, the cellulose was in a state of tension, which is, to our knowledge, the first experi- mental evidence supporting the assumption that tension is induced in cellulose micro- fibrils in the tension wood cell wall [1].

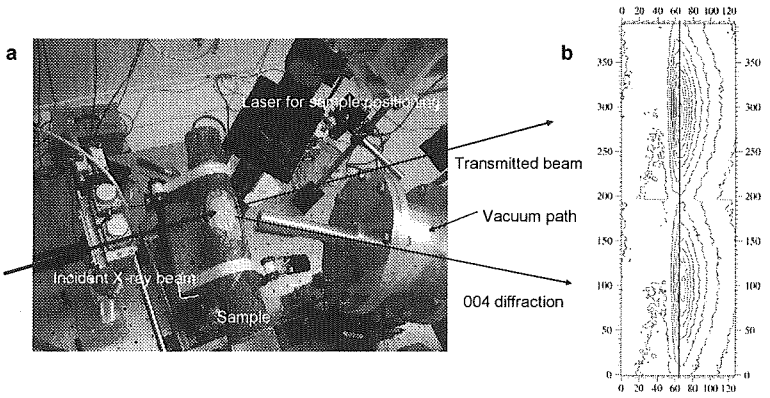

Fig 1 a: Experimental setup at BL40XU, SPring8, Harima, Japan. The log was tightly fixed being tilted ca.15° with respect to the incidence so that the (004) planes satisfy Bragg condition. The vacuum path of 1.5 m was inserted to suppress the background due to the air scattering.
b: The peak position of (004) diffraction shifted toward the higher angle (to the right), indicating that the fiber repeat distance is extended upon the release of the maturation stress.

[1] Clair B, Almeras T, Yamamoto H, Okuyama T, Sugiyama J, 2006, Biophys J, BioFAST: doi:10.1529/ biophysj.105.078485

Exclusive overexpression and structure-function analysis of a versatile peroxidase from white-rot fungus, *Pleurotus ostreatus*

(Laboratory of Biomass Conversion, RISH, Kyoto University)

Yoichi Honda, Takahito Watanabe and Takashi Watanabe

White-rot fungi play a critical role in the carbon cycle in arborsphere by degrading plant cell wall substances produced in photosynthesis. Especially, the unique ability to decompose a recalcitrant polymer lignin in a mild condition has advantages as a strong tool for conversion of biomass resources to useful materials including energy compounds and biodegradable plastics, by which the naturally-occurring system would function more extensively in carbon cycling within humanosphere. Toward the elucidation and application of the mechanism for lignin biodegradation, we are operating manifold approaches including biochemical, enzymological and molecular genetical methodologies.

Versatile peroxidases (VPs) are a family of peroxidases secreted by several white-rot basidiomycetes belonging to the *Pleurotus* and *Bjerkandera* genera and are considered to be the key enzyme in the lignin biodegradation system by these fungi. VPs are characterized for their extraordinary wide substrate specificity and retain features of the other two fungal peroxidase families, manganese peroxidases (MnPs) and lignin peroxidases (LiPs). Therefore, a highly efficient VP-overproduction system is desired for biotechnological applications in industrial processes and bioremediation of recalcitrant pollutants, and also detailed analysis of the structure-function relationship of the enzyme.

Although *Pleurotus ostreatus* MnP2 was earlier mentioned as a typical MnP isozyme, we reported that MnP2 can oxidize veratryl alcohol [1] and even high molecular-weight compounds such as RNase A and a polymeric azo dye Poly R-478 [2]. The deduced amino acid sequence from the cloned *mnp2* gene demonstrated that this isozyme contains the tryptophane residue (W170) conserved among LiPs and VPs. Chemical modification of purified MnP2 by *N*-bromsuccimide blocked the oxidizing activity for veratryl alcohol, RNase A and Poly R-478, suggesting that W170 plays an essential role in oxidizing these compounds [2]. Recently, genetically modified *P. ostreatus* strains with elevated MnP2 productivity were isolated by transforming an expression construct containing the coding region of *mnp2* under the control of a homologous *sdi1* promoter sequence [3]. *sdi1* encodes for Iron-sulphur protein subunit of succinate dehydrogenase, one of the components of the mitochondrial respiratory chain and the recombinant *mnp2* gene is expected to be transcribed constitutively. The recombinant strains exhibited enhanced Poly R-478-decolorizing and benzo[*a*]pyrene-removing activities [3], demonstrating their high potential as biocatalysts in biological processes. However, the production yield of the extracellular enzymes with Mn^{2+}-dependent peroxidase activity by the recombinants was at most 230 U/l in a stationary culture using a synthetic medium. Through optimization of the culture conditions, an exclusive expression of the recombinant MnP2, upto 7300 U/l, without background expression of endogenous MnP isozymes was achieved [4]. Using this system, MnP2 variants constructed with site-directed mutagenesis at W170 and its surrounding amino acid residues were successfully expressed and their catalytic activities for low and high molecular-weight substrates are being analyzed.

REFERENCES

[1] Kamitsuji, H., Honda, Y., Watanabe, T. and Kuwahara, M. (2004) Appl. Microbiol. Biotechnol., 65: 287-294.

[2] Kamitsuji, H., Watanabe, T., Honda, Y. and Kuwahara, M. (2005) Biochem. J., 386: 387-393.

[3] Tsukihara, T., Honda, Y. and Watanabe, T., (2006) Appl. Microbiol. Biotechnol., 71: 114-120.

[4] Tsukihara, T., Honda, Y. Sakai, R., Watanabe T. and Watanabe, T., (2006) J. Biotechnol., in press.

Targeted approaches in metabolic science of forest plants and microorganisms

(Laboratory of Metabolic Science of Forest Plants and Microorganisms, RISH, Kyoto University)

Toshiaki Umezawa and Takefumi Hattori

It is becoming more important to establish a sustainable society, which depends on renewable resources. Because wood biomass is the most abundant renewable resource, studies of wood formation is the key to improve forest biomass production. In this context, we are involved in analyzing metabolic functions of forest plants and microorganisms from a wide variety of aspects, including organic chemistry, biochemistry, molecular biology, and metabolomics, in order to conduct basic investigations contributing cultivation and protection of forest resources.

1. Molecular cloning of novel genes encoding enzymes of phenylpropanoid biosynthesis

In the post-genomic era, to understand mechanisms for metabolisms in forest plants and microorganisms, the integration of comprehensive or holistic analyses such as transcriptomics, proteomics and metabolomics and targeted analyses are critically important.

The cinnamate/monolignol pathway supplies precursors for various phenylpropanoid compounds such as lignins, lignans, and norlignans, which are involved in secondary xylem formation composed of cell-wall and heartwood formation of herbaceous and woody plants. The lignan pathway which follows the cinnamate/monolignol pathway is involved in heartwood formation and production of bioactive compounds. Thus, these pathways play central roles in plant secondary metabolism.

We have been working on comprehensive or network analysis of gene expression involved in secondary xylem formation. In addition, from the aspects of the targeted approach, we have cloned two novel genes. One is a novel *O*-methyltransferase (OMT) catalyzing methylation of a lignan, matairesinol, giving rise to arctigenin. This is the first example of molecular cloning of a cDNA encoding a lignan OMT. In addition, we have cloned cDNAs encoding a norlignan synthase, which catalyzes the formation of hinokiresinol from *p*-coumaryl *p*-coumarate. Both genes or their homologs are involved in heartwood formation, and these enzymes are can be used as clues to help us elucidate heartwood formation mechanisms.

2. Mechanisms for organic acid metabolism of wood-rotting fungi and ectomycorrhizal fungi

Biodegradation of wood components by wood-rotting (WR) fungi including white- and brown-rot basidiomycetes is important as a first process leading to humus production, which in turn contributes greatly to sustainable forest ecosystems. Oxalate excreted from WR fungi plays a wide variety of roles in the degradation owing to its various chemical natures. We have proposed that oxalate metabolism is an important biochemical device to produce energy for fungal growth of WR fungi. Firstly, we reported that oxalate decarboxylase and formate dehydrogenase play an important role in decomposing oxalate to produce NADH as an energy source during vegetative growth of white-rot fungus *Cereporiopsis subvermispora*. Secondly, we proposed that peroxisomal glyoxylate (GLOX) cycle cooperatively play a role with mitochondrial TCA cycle in oxalate fermentation by which brown-rot fungus *Fomitopsis palustris* acquires energy for fungal growth on glucose. To the best of our knowledge, this is a first example to show peroxisomal GLOX cycle in glucose-grown mycelia. Furthermore, it was postulated that in glucose-grown *F. palustris* some of the common metabolites of the peroxisomal GLOX and mitochondrial TCA cycles are transported between peroxisomes and mitochondria in a constitutive and cooperative manner in terms of the oxalate biosynthesis.

Cytochemical and molecular approaches for enzymes and transporters involved in organic acid metabolism are being investigated for WR fungi. Furthermore, comprehensive study for elucidation of regulatory mechanisms for organic acid metabolism in WR and ectomycorrhizal fungi has just begun.

Identification and characterization of *p*-hydroxybenzoate polyprenyltransferase gene involved in coenzyme Q biosynthesis in rice.

(Laboratory of Plant Gene Expression, RISH, Kyoto University)

Kazufumi Yazaki

Ubiquinone (UQ, coenzyme Q) is a lipid-soluble electron carrier required for the respiratory chain in the mitochondria of eukaryotic cells. Adding to the conventional clinical use for the improvement of heart function, UQ has also been recently used in cosmetics and food supplements to prevent the accumulation of active oxygen species.

Prenylation of the aromatic intermediate *p*-hydroxybenzoate (PHB) is a critical step in UQ biosynthesis. The enzyme that catalyzes this prenylation reaction is PHB polyprenyltransferase (PPT), which substitutes an aromatic proton at the *m*-position of PHB with a prenyl chain provided by polyprenyl diphosphate synthase. The rice genome contains three PPT candidates that share significant similarity with the yeast PPT (*COQ2* gene), and the rice gene showing the highest similarity with *COQ2* was isolated by RT-PCR and designated *OsPPT1a*. The deduced amino acid sequence of OsPPT1a contained a putative mitochondrial sorting signal at the N-terminus and conserved domains for putative substrate-binding sites typical of PPT protein family members. The subcellular localization of OsPPT1a protein was shown to be mainly in mitochondria based on studies using a green fluorescent protein-PPT fusion. A yeast complementation study revealed that *OsPPT1a* expression successfully recovered the growth defect of *coq2* mutant. A prenyltransferase assay using recombinant protein showed that OsPPT1a accepted prenyl diphosphates of various chain lengths as prenyl donors, whereas it showed strict substrate-specificity for the aromatic substrate PHB as a prenyl acceptor. The apparent K_m values for geranyl diphosphate and PHB were 59.7 and 6.04 μM, respectively. Their requirement by OsPPT1a for divalent cations was also studied, with Mg^{2+} found to produce the highest enzyme activity. Northern analysis showed that *OsPPT1a* mRNA was accumulated in all tissues of *O. sativa*. These results suggest that OsPPT1a is a functional PPT involved in UQ biosynthesis in *O. sativa*.

REFERENCE

Ohara, K., et al. *Plant Cell Physiol.* **47 (5):** 581-590 (2006)

Temperature and Humidity Monitoring with GPS Occultation and the Contribution to the Global Earth Observation System of Systems (GEOSS)

(Laboratory of Atmospheric Sensing and Diagnosis, RISH, Kyoto University)

Toshitaka Tsuda, Takuji Nakamura, and Takeshi Horinouchi

Last year (2005), we started a new 3-year research project "Temperature and Humidity Variability Analyses with GPS occultation" (project leader, T. Tsuda) funded by the Ministry of Education, Culture, Sports, Science and Technology (MEXT). In this document, we describe the background, overview, and current status of the project.

We have earlier conducted research projects under collaborations with many research organizations such as Japan Meteorological Agency (JMA), Meteorological Research Institute (MRI) under JMA, National Institute of Information and Communications Technology (NICT), Electric Navigation Research Institute (ENRI), American University Cooperation for Atmospheric Research (UCAR), and Brazilian National Institute for Space Research (INPE). In those projects, we have conducted studies to develop and utilize the GPS occultation technique. This technique is to measure atmospheric refractivity profiles using the path bending and phase delay of the radio waves transmitted from the Global Positioning System (GPS) satellites. The refractivity is then used to derive the humidity and temperature of the atmosphere. One of the many achievements of the projects is that it has been demonstrated that the GPS occultation can improve weather forecast. Also, it has been shown that the technique provides a unique opportunity to study the tropical and sub-tropical atmospheric phenomena that have fine vertical structures.

In order to further pursue these two features, we have started the present research project under collaboration with NICT and MRI. The entire funding, under which our project is supported, is aimed at constructing the Global Earth Observation System of Systems (GEOSS) proposed multilaterally in the Earth Observation Summit. The "System of Systems" indicates its strategy to closely coordinate distributed efforts for better environmental monitoring.

Our project consists of three sub-projects and can be summarized as follows: we will (1) develop new retrieval techniques with NICT, (2) assimilate GPS occultation in regional weather forecast models with MRI, and (3) validate and scientifically analyze the occultation measurements.

In sub-project (1) NICT has been developing a full-spectral inversion code, which will improve the accuracy of refractivity retrievals. In sub-project (2) MRI has been developing new assimilation techniques and has demonstrated the improvement of the regional forecast. In sub-project (3), we are making observational validations and scientific analyses of the atmosphere in the tropics and Asian monsoon region. Also, we are developing a new technique to integrate GPS occultation data. This is to process the data from COSMIC/FOMOSAT-3 constellational observation, in which recently-launched six satellites will provide unprecedented high-frequency, high-spatial-density atmospheric soundings. The data will be expected to significantly improve weather forecasts and monitoring of the Earth's atmosphere. Figure 1 shows a map of expected global distribution of GPS occultation measurements in 24 hours. One can see the very high observation density from this figure.

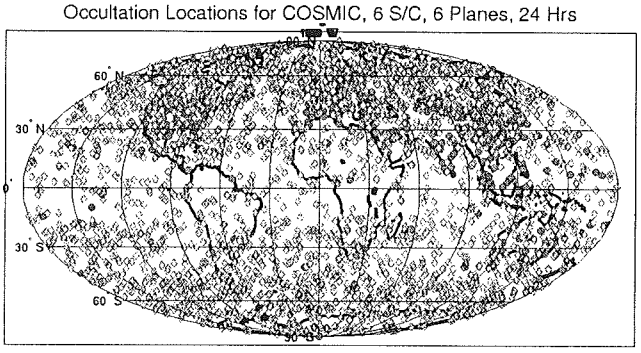

Figure 1. Expected GPS occultation events within 24-hours with COSMIC/FOMOSAT-3 GPS occultation measurements.

Coupling Study of Mid-latitude *E*- and *F*-region Irregularities over Japan

(Laboratory of Atmospheric Environment Information Analysis, RISH, Kyoto University)

Mamoru Yamamoto

Various types of plasma instabilities have been studied in the mid-latitude ionosphere *E*- and *F*-region. Field Aligned Irregularities (FAIs) in both regions is one of them. The *E*-region FAI (E-FAI) is caused by the polarization electric field in the electronic density perturbation of the Sporadic *E* layer. The *F*-region FAI (F-FAI) is generated by the polarization electric field at the wall of the Traveling Ionosphere Disturbances (TID). In the ionosphere, conductance parallel to the geomagnetic filed is so high that such polarization electric fields are easily mapped along the field line for several hundred kilometers. Because of these characteristics, electromagnetic coupling is expected between the *E*- and *F*-region. We studied ionospheric *E*- and *F*-region coupling process from the FERIX (*F*- and *E*- Region Ionosphere Coupling Study) campaign in 2004, and from statistical comparison of radar observation of E-FAI and the GPS-TEC perturbation over Shigaraki in 2005.

During the FERIX campaign, we used the MU radar and LTPR (Lower Thermosphere Profiler Radar) located in Sakata, Yamagata for simultaneous observations of *F*- and *E*-region FAIs, respectively (Fig. 1). We successfully found the coupling of E-FAI and F-FAI that occurred along the same magnetic field lines (Fig.2). The horizontal structures of E-FAI, F-FAI and TID are all aligned from northwest to southeast, and propagated to the west at the same speed. From the statistical analysis, the coupling was often detected when the TID had a northwest-southeast wavefront structure.

From these results, we found several direct evidences of electromagnetic coupling between the *E*- and the *F*-regions. When the coupling is observed, northwest-southeast aligned structures were often seen in both regions. This is consistent with the theoretical study by Cosgrove *et al.* [2004]. On the other hand, when the *E*- and *F*-regions don't couple, the QP structures of E-FAI seem to occur only by the gravity wave or Kelvin-Helmholtz instability in the neutral atmosphere.

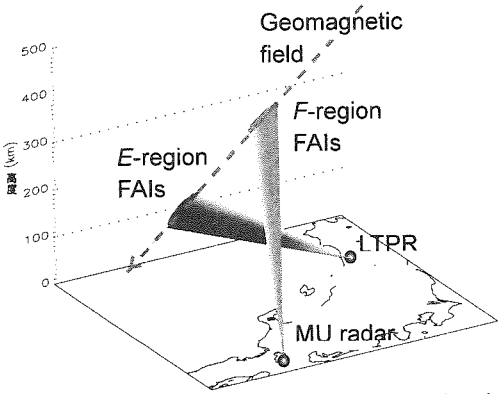

Fig. 1: Configuration for FERIX campaign in 2004. The MU radar and LTPR observe F- and E-region FAI echoes, respectively, along the same geomagnetic field line.

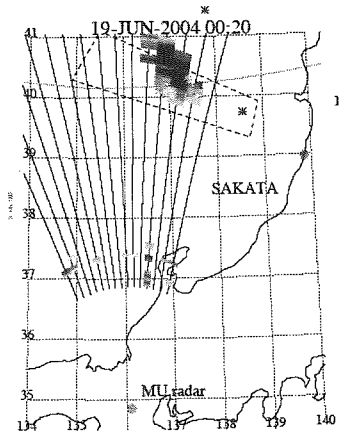

Fig. 2: Horizontal distribution of echoed from F-FAI (shade) and E-FAI (dots). F-FAI echoes are mapped down to 100km altitude along the geomagnetic field.

REFERENCE

Cosgrove, R. B., R. T. Tsunoda, S. Fukao and M. Yamamoto, Coupling of the Perkins instability and the sporadic E layer instability derived from physical arguments, J. Geophys. Res., 109, A06301, doi:10.1029/2003JA010295, 2004.

Cirrus cloud observation in the tropical upper troposphere by the Equatorial Atmosphere Radar (EAR) and 95-GHz cloud radar

(Laboratory for radar atmospheric sciences, RISH, Kyoto University)

Shoichiro Fukao, Hiroyuki Hashiguchi, and Masayuki K. Yamamoto

Cirrus clouds are high- and thin-tropospheric clouds composed predominately of ice particles. Tropical cirrus clouds cover a significant part of the tropics and have a key effect on the Earth's radiation budget. They occupy an area much greater than the deep convection that produces them. Modeling and observational studies have been carried out to understand the complete life cycle of tropical cirrus clouds and basic processes responsible for their persistence. However, observational studies on the interactions among radiation, dynamics, and microphysics remain too sparse. Especially, dynamical processes of tropical cirrus clouds are not understood well, because wind observation in and around tropical cirrus clouds with high temporal and vertical resolution has not been carried out.

A VHF-band wind profiler called the Equatorial Atmosphere Radar (EAR) can observe winds in both clear and cloudy regions by receiving echoes from atmospheric turbulence [1]. A 95-GHz cloud radar can detect ice particles within cirrus clouds due to its short wavelength (3.2 mm) [2]. Therefore, the combination of the EAR and the 95-GHz cloud radar enables us to observe fine wind structure in and around cirrus clouds. In November 2005, our research group has carried out the observation campaign using the EAR and 95-GHz cloud radar to understand how background wind affects dynamical and microphysical processes of cirrus clouds. The observation campaign was carried out as a joint project by RISH and National Institute of Information and Communications Technology (NICT). The 95-MHz cloud radar is installed close to the EAR at the Equatorial Atmosphere Observatory (0.2S, 100.32E, 865 m above sea level) near Bukittinggi, West Sumatra, Indonesia.

From the preliminary data analysis, our research group has already obtained several new findings: a linkage between falling velocity of ice particles and background vertical air motion, enhanced turbulence near the cloud bottom caused by evaporative cooling, and so on. Other than the EAR and the 95-GHz cloud radar, many instruments such as weather radars, lidar, and radiosondes were under operation during the observation campaign. Using these data, the dynamical and microphysical processes of tropical cirrus clouds will be further investigated.

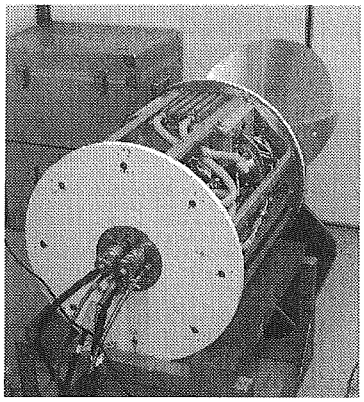

Figure 1: Picture of the 95-GHz cloud radar

Figure 2: A view of the EAR

REFERENCES

[1] Fukao, S., Hashiguchi, H., Yamamoto, M., Tsuda, T., Nakamura T., Yamamoto M. K., Sato, T., Hagio, M., and Yabugaki. Y. (2003), Radio Sci., 38(3), 1053, doi:10.1029/2002RS002767.

[2] Horie, H., T. Iguchi, H. Hanado, H. Kuroiwa, H. Okamoto, H. Kumagai (2000), IEICE TRANS. COMMUN., 83, 2010-2020.

Interactions between cellulose chains and waters

(Laboratory of active bio-based materials, RISH, Kyoto University)

Fumio Tanaka

Most of the structural studies of cellulose have been based on the crystallographic data obtained by diffraction measurements under the waterfree dried environment. So the highly crystalline state of cellulose has been obtained from the measurements. Then, the cellulosics were interpreted to be stiff and rigid materials. However, cellulose molecules originally exist with waters in biosystem. The dried state cellulose must be a kind of artificial material. Is the conventional argument for cellulose until now adequate to discuss the physical properties of cellulosic material? Then, we investigated the characteristics of cellulose in aqueous conditions by molecular simulation technique.

The threedimensional features of cellulosic aggregates in aqueous conditions were simulated as a model of cellulose in biosystem ((3) and (4) in the Figure) compared with those in nonaqueous state ((1) and (2) in the Figure). Cellulose chains in aqueous environment were found to have no direct hydrogen bondings between the chains. Most of hydrogen bondings in the cellulosic aggregates were formed through waters in aqueous state. This situation was not changed after the optimization process. The new hydrogen bonding between cellulose chains directly was not formed in aqueous conditions even after the optimization process. This meant that waters were preventing to form hydrogen bondings directly between cellulose chains. This feature showed the low crystallinity of cellulose in green conditions. The low crystallinity of cellulose was observed in fact from the plant specimens in green conditions. On the other hand, the cellulose chains in nonaqueous environment approached each other very quickly and formed the hydrogen bondings directly between them. This was a tight aggregate like a crystal.

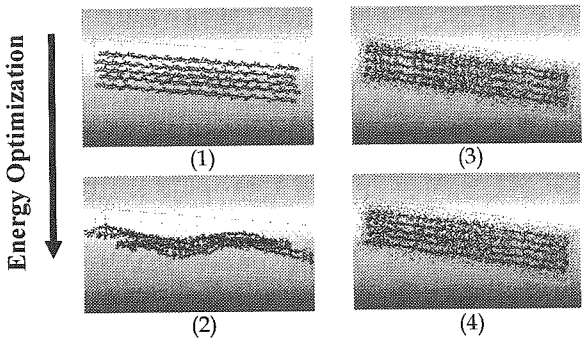

Interactions between cellulose chains and waters. (1) and (2) showed in non-aqueous state. (3) and (4) showed in aqueous state. (1) and (3) showed pre-optimization state. (2) and (4) showed after-optimization state.

The highly crystalline materials are stiff and strong, but a little bit brittle. On the contrary, low crystalline materials are a little bit flexible. Above is the reason why the green tree is more resilient than the dried wood.

REFERENCES

[1] Tanaka, F. and Fukui, N. 2004. *The behavior of cellulose molecules in aqueous environments*, Cellulose 11:33-38.

[2] Tanaka, F. and Okamura, K. 2005. *Characterization of cellulose molecules in bio-system studied by modeling methods*. Cellulose 12:243-252.

Durability of P-MDI Adhesive Exposed to Ultraviolet Rays

(Laboratory of Sustainable Materials, RISH, Kyoto University)

Kenji Umemura

Formaldehyde emission from wood products utilizing formaldehyde resin adhesives has become a public concern. Recently, polymeric diphenylmethane diisocyanate (P-MDI) have been used gradually as a non-formaldehyde wood adhesive. Accordingly, the durability and degradation of P-MDI when used as a wood adhesive has become of interest. Generally, heat and moisture are thought to be the most important degradation factors for the durability of wood adhesives. The durability and degradation mechanism of P-MDI have been investigated concerning the degradation factors. Besides those factors however, various degradation factors would be acting in actual environment. Especially, P-MDI can be used as an adhesive for material surface such as overlay in recent years. In this case, P-MDI seems to be greatly affected by ultraviolet rays (UV). We investigated the effect of UV on durability of P-MDI.

First, water was added to an aqueous emulsion type P-MDI at an NCO/OH ratio of 0.5. The mixture was blended by vigorous stirring, and was applied to a bakelite plate (6×11×0.1cm). The plate was cured at 40°C for 24hr. As a wood specimen, Japanese cedar (*Cryptomeria japonica*) solid wood was used. The specimens were irradiated with UV in a UV long life fade meter. After irradiation, the surface color, chemical and mechanical properties were observed. As a control, the specimens were treated at the same temperature and humidity without UV.

Figure 1 shows the color changes of solid wood under UV irradiation. The color changed slightly to dark with increasing irradiation time. On the other hand, Figure 2 shows the color changes of cured PMDI. The color changed to dark drastically in short irradiation time and then reached an almost constant dark color. When the treatment without UV irradiation was performed, the color of cured PMDI did not changed so much. A similar trend was also observed for the wood. Based on the results obtained, it was clarified that the color of cured PMDI was drastically changed by UV in a short time. Therefore, when PMDI is used in material surface, it is necessary to pay attention to the color change. According to FT-IR measurement and dynamic mechanical analysis however, the degradation of main chemical structure and the lowering of mechanical properties were hardly observed. Now, we are performing the exterior exposure test to clarify the detail durability of P-MDI.

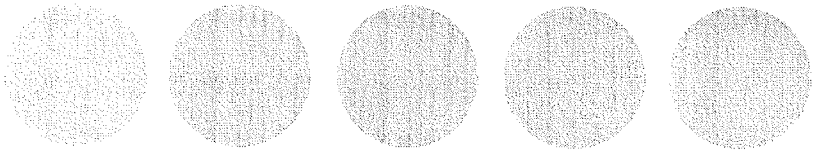

Fig.1. Color changes of Japanese cedar irradiated with UV light.

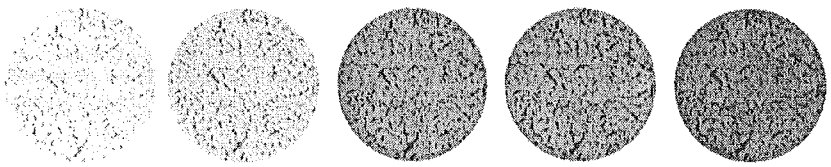

Fig.2. Color changes of cured PMDI irradiated with UV light.

Development of Ductile and High-Strength Semi-Rigid Portal Frame Composed of Mixed-Species Glulams and H-shaped Steel Gusset Joints

(Laboratory of Structural Function, RISH, Kyoto University)

Kohei Komatsu and Takuro Mori

Recent in Japan, demands for glulam portal frames to be used in wooden residential houses are increasing. These portal frames are expected to have a function as the structural component, which can sustain not only vertical loads but also lateral load due to wind or/and earthquake load.

Generally speaking, however, portal frame structures are inferior to nailed-on-sheathed shear wall structures in the aspect of strength performance. Thus, in order to develop the glulam portal frames usable in wooden residential house instead of shear walls, it will be most important to improve the strength performance of the portal frames up to the level same as that of shear walls.

By setting this level of structural performance as the target of research & development, we and some company's researcher tried to improve the strength performance of glulam portal frame by paying attentions to the selection of best assembly with materials and connection. Figure 1 shows the combination of the materials and connection. These materials are a mixed-species glulam members, in which relatively low MOE and soft quality Sugi (*Cryptomeria japonica* D.Don) was used for the inner members while high MOE and hard quality Douglas-fir (*Pseudotsuga menziesii*) was used for the outer part of glulam. This connection is steel gusset plate having flanges like H-shape steel member. In the steel gusset plate joint, the load transmission was intended to be done though the stronger laminations by means of steel flanges.

The newly developed portal frames are tested. Testing method and the detail of the materials showed in figure 2. We have 4m and 6m span lengths. As results, figure 3 shows the load-shear deformation angle on the 6m span specimen. It gave a ductile and high-strength semi-rigid glulam portal frame. It can reveal 1.9 shear resistance factor per unit meter, which implies that there is not only an equivalent shear wall having shear resistance factor of 1.96kN times 1.9 allowable strength per unit meter but also an opened space of 6m span.

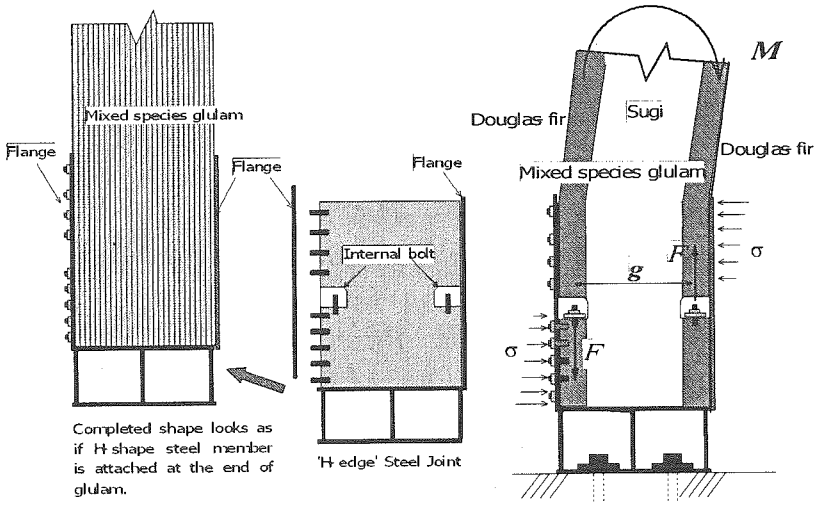

Fig. 1. Best combination of the mixed species glulam and newly developed flange-type steel gusset joint with internal bolts.

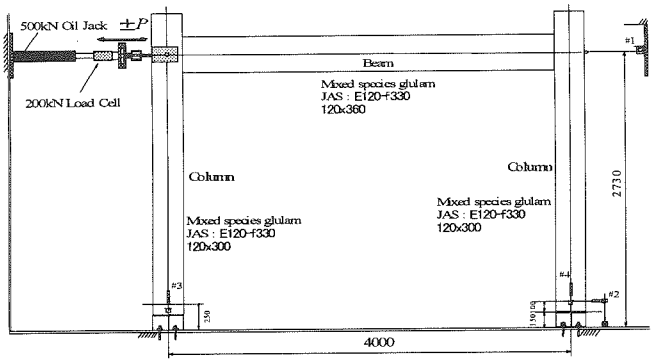

Fig. 2. Test set-up for full-scale glulam portal frame specimen.

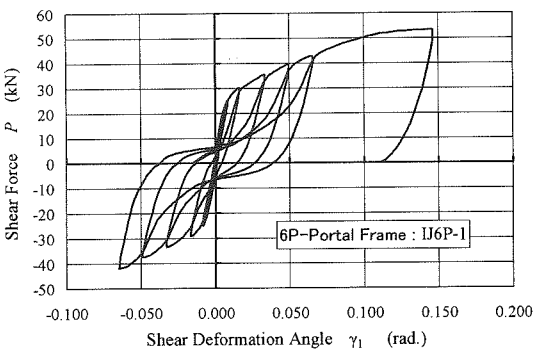

Fig. 3. Example of load (P)-shear deformation angle (γ) for 6P specimen.

Feeding ecology of the invasive dry-wood termite *Incisitermes minor* (Hagen) in Japan

(Laboratory of Innovative Humano-Habitability, RISH, Kyoto University)

Yuliati Indrayani and Tsuyoshi Yoshimura

One of the important wood-destroying insect groups in the world is the dry-wood termite. Dry-wood termites are considered serious threats to wooden structures and wood products. One of the dry-wood termite species categorized as a serious pest in the United States is the western dry-wood termite, *Incisitermes minor* (Hagen). Colonies of *I. minor* were found in both natural and man-made environments and live entirely within sound dry wood. Due to these ecological characteristics, *I. minor* is easily transported in infested wood products by various human activities. Japan is one of the major countries importing wood and wood-based materials that can serve as a natural habitat of *I. minor*. This exotic species has been reported in a number of locations in Japan and appears to be spreading these days [1] [2].

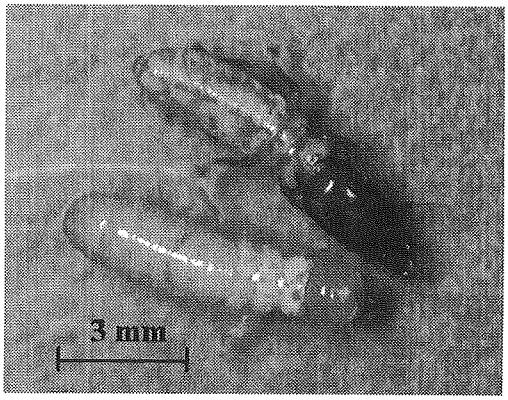

Figure 1: Worker and soldier of *Incisitermes minor* (Hagen)

To identify the parentage assessment of *I. minor* distributed in Japan, ten polymorphic microsatellite markers were developed by using a genomic DNA extracted from the heads of workers. We have successfully obtained the individual DNA structure of *I. minor*, and that *I. minor* distributed in Japan had close genetic relationship with *I. minor* distributed in California, USA [3].

The roofing materials such as rafters, eaves, gables, boards, and beams were the most susceptible parts by *I. minor*. Interior materials such as pillars, window and door frames, thresholds, lintels, floor boards, and tatami, and exterior materials such as wall boards, beams, braces, window frame, and thresholds were the second-most frequently attacked parts as well [4].

I. minor was reported to be much more tolerant against high temperatures and arid conditions when compared to other termite species. Temperature and humidity are likely to play important roles in the survival of termites and influences their feeding activities. The optimal temperature and RH conditions for the feeding activities were 35°C and 70%, respectively, and the optimal combinations were 35°C-70% and 35°C-80%. The hottest temperature (40°C) caused termites to become moribund, and their feeding activity decreased rapidly. The coolest temperature (15°C) did not kill the termites, but did reduce the feeding activity [5].

Lastly, we determine the resistance of ten commercial wood species commonly used in Japan against *I. minor* such as five Japanese timbers, four U.S. timbers and one Malaysian timber. The ranking of the resistance of the ten commercial timbers against *I. minor* was buna>karamatsu>sugi>western red cedar>Douglas fir>rubber>western hemlock>hinoki>spruce [6].

REFERENCES

[1] Indrayani, Y., Yoshimura, T., Fujii, Y., Yanase, Y., Okahisa, Y., Imamura, Y. (2004) Jpn. J. Environ. Entomol. Zool., 15:261-268

[2] Mori, H. (1976) *Shiroari* (*Termite*), 27:45-47 (in Japanese)

[3] Indrayani, Y., Matsumura, K., Yoshimura, T., Imamura, Y., Itakura, S. (2006) Molecular Ecology Notes, *in press*

[4] Indrayani, Y., Yoshimura, T., Fujii, Y., Yanase, Fujiwara, Y., Adachi., A., Kawaguchi, S., Miura, M., Imamura, Y. (2005) Sociobiology, 46:45-63

[5] Indrayani, Y., Yoshimura, T., Fujii, Y., Yanase, Imamura, Y. (2006) J. Wood Sci., *in press*

[6] Indrayani, Y., Yoshimura, T., Imamura, Y. (2005) Proceeding of The 6th International Wood Science Symposium, Bali, Indonesia, 33

Numerical Analysis on Microwave Beam Interaction with Ionospheric Plasma in Space Solar Power System

(Laboratory of Computer Simulations for Humanospheric Science, RISH, Kyoto University)

Hideyuki Usui and Yoshiharu Omura

In the Space Solar Power System (SSPS, Fig. 1), solar energy is converted to microwaves and transmitted to the ground. In order to study the feasibility and the implications of SSPS, we conducted several rocket experiments of microwave power transmission (MPT) in the ionosphere. In the rocket experiments, we found that electrostatic plasma waves were excited around the local plasma frequency in association with intense microwave emission. This plasma interaction may cause the loss of microwave energy. Theoretical analysis showed that the excited electrostatic waves are due to so called three-wave coupling. In order to study the nonlinear wave-wave-particle interaction associated with the microwave energy transmission in space plasma, we performed numerical simulations with an electromagnetic PIC (Particle-In-Cell) model. In the simulations, we focus on the spatial and temporal evolution of the three-wave coupling as well as the dependence of the interaction on the amplitude of the pump electromagnetic waves.

In the simulation space filled with magnetized plasma, we emit intense electromagnetic waves from an antenna located at one edge of the simulation system. When the electromagnetic waves are intense enough, a three-wave coupling occurs, which is the consequence of a nonlinear interaction between forward and backward propagating high-frequency electromagnetic waves and a low-frequency electrostatic one propagating in the forward direction. The results show that a fraction of the electromagnetic waves emitted from the antenna is backscattered by the background plasma, which induces electrostatic waves at the plasma frequency (fig. 2). Since the electrostatic waves cause electron heating, the local plasma condition changes and the three-wave coupling ceases.

We also found that the nonlinear process can be affected by the local electron heating by the excited electrostatic waves because the characteristics of the excited waves depend on the electron temperature. When the geomagnetic field is perpendicular to the microwave propagation, electrons are most heated because the excited electron cyclotron harmonic waves are less affected by the electron temperature.

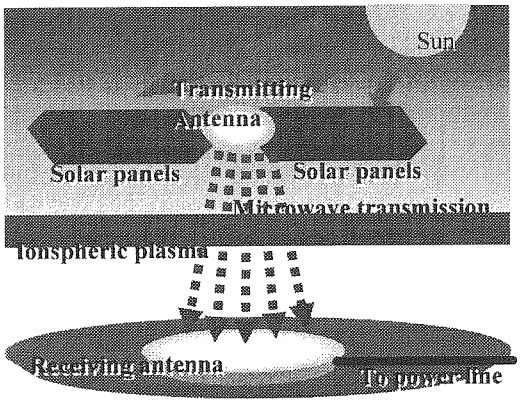

Fig.1 SSPS (Space Solar Power System)

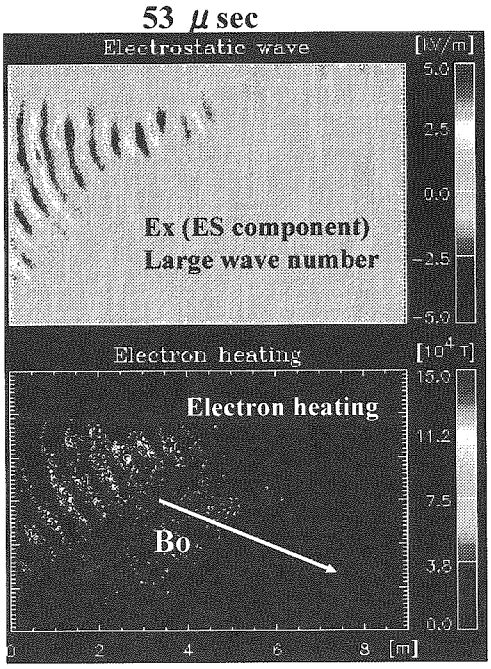

Fig. 2 Two dimensional simulation results which show low frequency electrostatic wave excitation (upper panel) and associated electron heating (lower panel).

REFERENCE

Usui, H., H. Matsumoto, and R. Gendrin, Numerical simulations of a three-wave coupling occurring in the ionospheric plasma, Nonlinear Processes in Geophysics, Vol.9 No. 1, 1-10, 2002.

A fundamental study of a microwave pretreatment system for wood biomass conversion

(Laboratory of Applied Radio Engineering for Humanosphere, RISH, Kyoto University)

Tomohiko Mitani, Naoki Shinohara and Kozo Hashimoto

Microwave heating is one of the microwave applications close to our daily life, as typified by a microwave oven. While conduction heating can only reach the surface of a material, microwave heating can reach the inside of a material directly and uniformly, hence it spends less time heating.

Microwave heating is also known as one of effective pretreatment methods for converting wood biomass into bio-ethanol (*e.g.* [1]). The objective of the present study is to develop a microwave pretreatment system for wood biomass. The microwave pretreatment system requires (1) high DC-microwave conversion efficiency, (2) high heating efficiency, (3) short heating time, (4) productivity per time, electric power and cost, etc.

A fundamental design study on a container for a microwave pretreatment system is currently being conducted. The container is designed with 3D electromagnetic simulator called HFSS (High Frequency Structure Simulator). Fig. 1 shows the simulation results of cross-sectional electric field distribution in a container at a frequency of 2.45GHz. The difference between Fig. 1(a) and Fig. 1(b) is the container size. From these results, electric field intensity is uniformly strong inside as shown in Fig. 1(a); whereas it is uneven in the center of the container as shown in Fig. 1(b). Therefore, the container size of Fig. 1(a) is more effective for microwave heating than that of Fig. 1(b). The results also indicate that a slight change of the container size greatly affects electric field distribution.

For future works, a design study on a container with high overall efficiency will be conducted at a frequency of 5.8GHz as well as 2.45GHz.

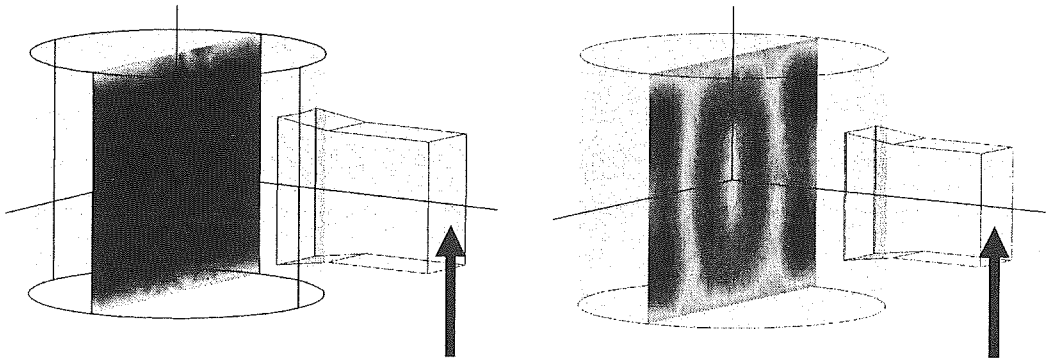

(a) diameter:250mm, height 200mm (b) diameter:300mm, height 250mm

Fig. 1. Simulation results of cross-sectional electric field distribution in a container for a microwave pretreatment system at a frequency of 2.45GHz. The dark color shows that electric field intensity is strong there.

REFERENCES

[1] Azuma, J., F. Tanaka and T. Koshijima, "Microwave Irradiation of Lignocellulosic Materials I –Enzymatic susceptibility of microwave-irraditated woody plants-", Mokuzai Gakkaishi Vol.30, No.6. pp.501-509, 1984

Plasma wave investigation in Mercury magnetosphere

(Laboratory of space radio science, RISH, Kyoto University)

Hiroshi Matsumoto, Hirotsugu Kojima, and Yoshikatsu Ueda

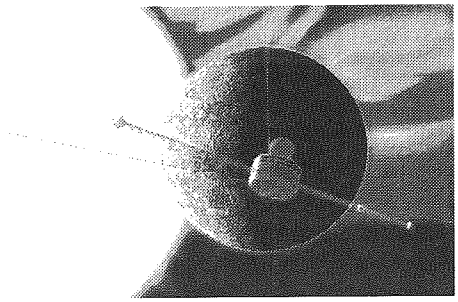

Figure 1: Mercury Magnetospheric Orbiter(MMO) of the BepiColombo mission (Artistic impression illustrated by C. Noshi.).

Mercury is the closest planet to the Sun. It is characterized by the highest density of all planets, very rarefied atmosphere and very weak intrinsic magnetic fields. Only American probe Mariner 10 has returned data from Mercury. It made three flybys of Mercury in 1974-1975 and obtained images of its surface and measured the plasma environments in Mercury. One of the most significant results in Mariner 10 mission to Mercury is to discover its intrinsic magnetic fields. Further, the data suggest the unexpected existence of the magnetosphere. However, the data in only three flybys of Mariner 10 are insufficient for revealing the features of this mysterious planet.

ESA (European Space Agency) and JAXA (Japan Aerospace exploration Agency) started the new mission to Mercury called "BepiColombo mission" under their collaboration. The BepiColombo mission consists of two independent spacecraft. They are the MPO(Mercury Planetary Orbiter) and MMO(Mercury Magnetospheric Orbiter). JAXA is responsible for developing the MMO spacecraft, which has the objective to investigate the Mercury magnetosphere.

To meet the scientific objectives of BepiColombo/MMO, we proposed the plasma wave receiver system called PWI (Plasma Wave Investigation) to the Announce of Opportunity issued by JAXA. Fortunately, JAXA selected and approved our proposal in November, 2004. We made a start for the detailed design of PWI. PWI is developed under the collaborations of Japanese and European scientists (Principal Investigator (PI): Hiroshi Matsumoto, Kyoto Univ.). The composition of PWI is summarized in Table 1.

PWI will address a wealth of fundamental scientific questions pertaining to the magnetosphere and exosphere of Mercury, the solar wind at Mercury location and solar radiation from the view point of Mercury. Together, these measurements will provide ample new information on the structure of the Herman magnetosphere as well as on its dynamics. New knowledge will be gained about energy transfer and scale coupling. We will learn more about wave-particle interactions in the Herman plasma environment. The MMO spacecraft is scheduled for launch in 2012.

Table 1: Composition of Plasma Wave Investigation

Sensors

Component	Frequency	Development/ Responsibility
WPT	*E*: 0Hz – 10MHz	Japan
MEFISTO	*E*; 0Hz – 10MHz	Sweden
LF-SC	*B*: 0Hz – 20kHz	Japan
DB-SC	*E*: 0Hz – 20kHz *B*: 20kHz – 640kHz	France

Receivers

Component	Frequency	Data	Development/Responsibility
EWO	*E*: 0Hz – 120kHz *B*: 0Hz – 20kHz	Spectrum/Wave-Form /Spacecraft Potential	Japan
SORBET	*E*: 2.5kHz – 10MHz *B*: 2.5kHz – 640kHz	Spectrum/Electron temperature	France
AM^2P	< 120kHz	Antenna impedance	France

Onboard software: Japan and Hungary

Functional analyses and metabolic engineering of plant prenyltransferase genes

Kazuaki Ohara

Laboratory of Plant Gene Expression, RISH, Kyoto University

Ubiquinone (UQ) is a lipid-soluble electron carrier in the respiratory chain. It mediates electron transfer from NADH dehydrogenase (Complex I) to succinate dehydrogenase (Complex II) and further to the bc1 complex (Complex III) at the inner mitochondrial membrane (1). In humans, cellular UQ contents, particularly in heart cells, peak at age 20 then decreases (2). UQ therefore has been efficacious as a medicine to improve heart function. UQ supplementation recently has been reported to have mild symptomatic benefits for patients with Alzheimer (3), Parkinson (4), and Huntington (5) diseases. Furthermore, food supplements and cosmetics that contain UQ as an antioxidative have become very popular in the world market. However, only little is known about its physiological role *in planta*.

UQ is distributed in various compartments as well as in the mitochondria; the nucleus, plasma membrane, Golgi vesicles, and lysosomes, in which UQ is thought to function as an antioxidant (6) or an electron transporter (7). In yeast and arabidopsis, UQ biosynthesis is believed to take place in the mitochondria, but there are reports of UQ biosynthesis in such other subcellular areas as the endoplasmic reticulum (ER) and the Golgi apparatus in both rat liver (8) and spinach (9). A key reaction step in UQ biosynthesis is the prenylation of *p*-hydroxybenzoate (PHB); i.e., coupling of the aromatic substrate and isoprenoid chain, which is presumed to be rate-limiting for UQ production (Fig. 1). PHB: polyprenyltransferases (PPT) which catalyze this reaction are membrane-bound proteins. These occur widely from bacteria to humans and form a gene family. The length of the isoprenoid side chain varies with the organism. For example, *Saccharomyces cerevisiae* has UQ6, *Escherichia coli* UQ8, and *Schizosaccharomyces pombe* UQ10 as does humans. UQ chain length specificity reportedly is determined by the product specificity of prenyldiphosphate synthase (10), whereas PPTs have broad substrate specifity for prenyldiphosphates of different chain lengths (11). One reported exception is the LePGT involved in the biosynthesis of shikonin, a red naphtoquinone secondary metabolite in boraginaceous plants. It recognizes solely geranyldiphosphate as the prenyl substrate (12).

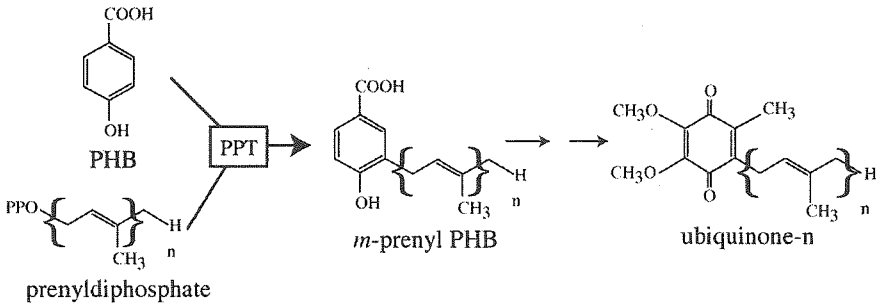

Fig. 1. Ubiquinone biosynthesis. PHB; *p*-hydroxybenzoate, PPT; PHB: polyprenyltransferase, *m*-prenyl PHB; *m*-prenyl-*p*-hydroxybenzoate.

The UQ contents in crop plants should be of interest in agricultural and food sciences, since this endogenous antioxidant may be quite beneficial for both consumers and producers, and thus the establishment of crops that produce UQ at high levels may be a new target of metabolic engineering. However, there has been no previous biosynthetic studies of UQ in crop plants, and therefore no biosynthetic gene is known, even in rice, which is both a model plant and a major crop that is cultivated worldwide. Moreover, the enzymatic properties of the PPT protein family have not been well characterized thus far. In this study, we characterized the *OsPPT1a* gene that encodes a rice PPT to clarify its biochemical properties as the key enzyme for UQ biosynthesis in rice. The deduced amino acid sequence of OsPPT1a contained a putative mitochondrial sorting signal at the N-terminus and conserved domains for putative substrate-binding sites typical of PPT protein family members. The subcellular localization of OsPPT1a protein was shown to be mainly in mitochondria based on studies using a green fluorescent protein-PPT fusion. A yeast complementation study revealed that *OsPPT1a* expression successfully recovered the growth defect of *coq2* mutant. A prenyltransferase assay using recombinant protein showed

that OsPPT1a accepted prenyl diphosphates of various chain lengths as prenyl donors, whereas it showed strict substrate-specificity for the aromatic substrate PHB as a prenyl acceptor. The apparent K_m values for geranyl diphosphate and PHB were 59.7 and 6.04 μM, respectively. Their requirement by OsPPT1a for divalent cations was also studied, with Mg^{2+} found to produce the highest enzyme activity. Northern analysis showed that *OsPPT1a* mRNA was accumulated in all tissues of *O. sativa*. These results suggest that OsPPT1a is a functional PPT involved in UQ biosynthesis in *O. sativa* (13).

In addition, we overexpressed the yeast *coq2* gene, which encodes PHB: hexaprenyltransferase (14), in order to increase the UQ10 content of tobacco. Because of the broad substrate specificity of COQ2, enhanced production of UQ10, which is native in tobacco, is to be expected because this enzyme functions as 'PHB: decaprenyltransferase' in tobacco. The COQ2 polypeptide deduced from the DNA sequence has a putative mitochondrial signal peptide at the N-terminus, as predicted by targetP (http://www.cbs.dtu.dk/services/TargetP/). In higher plants, however, little is known about the subcellular compartment of UQ biosynthesis. We engineered the subcellular localization of COQ2 in order to clarify whether there is mitochondrial or ER localization of this UQ biosynthetic enzyme by estimating its contribution to UQ production. The tobacco transgenic lines showed about a 6- fold increase in ubiquinone. COQ2 polypeptide, whose localization was enforcely altered to the endoplasmic reticulum, had the same or a greater effect as mitochondria-localized COQ2 on the increase in ubiquinone in both the yeast and tobacco transformants, indicative that the ubiquinone intermediate is transported from the endoplasmic reticulum to the mitochondria. Plants with a high ubiquinone level are more resistant to oxidative stresses caused by methyl viologen or high salinity. This is attributable to the greater radical scavenging ability of the transgenic lines as compared to the wild type (15).

REFERENCES

[1] Kroger, A., and Klingenberg, M. (1973) Eur J Biochem 39(2): 313-323
[2] Kalen, A., Appelkvist, E. L., and Dallner, G. (1989) Lipids 24(7): 579-584
[3] Grundman, M., and Delaney, P. (2002) Proc Nutr Soc 61(2): 191-202
[4] Muller, T., Buttner, T., Gholipour, A. F., and Kuhn, W. (2003) Neurosci Lett 341(3): 201-204
[5] Ferrante, R. J., Andreassen, O. A., Dedeoglu, A., Ferrante, K. L., Jenkins, B. G., Hersch, S. M., and Beal, M. F. (2002) J Neurosci 22(5): 1592-1599
[6] Stocker, R., Bowry, V. W., and Frei, B. (1991) Proc Natl Acad Sci U S A 88(5): 1646-1650
[7] Sun, I. L., Sun, E. E., Crane, F. L., and Morre, D. J. (1990) Biochem Biophys Res Commun 172(3): 979-984
[8] Kalen, A., Appelkvist, E. L., Chojnacki, T., and Dallner, G. (1990) J Biol Chem 265(2): 1158-1164
[9] Swiezewska, E., Dallner, G., Andersson, B., and Ernster, L. (1993) J Biol Chem 268(2): 1494-1499
[10] Okada, K., Suzuki, K., Kamiya, Y., Zhu, X., Fujisaki, S., Nishimura, Y., Nishino, T., Nakagawa, T., Kawamukai, M., and Matsuda, H. (1996) Biochim Biophys Acta 1302(3): 217-223
[11] Suzuki, K., Ueda, M., Yuasa, M., Nakagawa, T., Kawamukai, M., and Matsuda, H. (1994) Biosci Biotechnol Biochem 58(10): 1814-1819
[12] Yazaki, K., Kunihisa, M., Fujisaki, T., and Sato, F. (2002) J Biol Chem 277(8): 6240-6246
[13] Ohara, K., Yamamoto, K., Hamamoto, H., Sasaki, K., and Yazaki, K. (2006) Plant and Cell Physiol (in press)
[14] Ashby, M. N., Kutsunai, S. Y., Ackerman, S., Tzagoloff, A., and Edwards, P. A. (1992) J Biol Chem 267(6): 4128-4136
[15] Ohara, K., Kokado, Y., Yamamoto, H., Sato, F., and Yazaki, K. (2004) Plant J 40: 734-743

Wood-Based Sandwich Panel with Low-Density Fiberboard for use as Structural Insulated Wall and Floor

Tamami Kawasaki

Laboratory of Sustainable Materials, RISH, Kyoto University

INTRODUCTION Ever-increasing attention has been directed to the safer and more comfortable houses against the fear of nature, such as earthquake and global warming trend. Recent years have seen dramatic developments in the applications of wood-based materials as construction materials. Wood has attractive appearances inherent in biomaterial features, and excellent functional characteristics as a construction material such as stiffness, lightweight, and thermal insulation. The potential of wood as a building material and the need for the advanced use of wood as a sustainable material insure that the wood-based materials will continue to be in demand for the progressed human habitat style.

In dwelling house, the non-steady-state insulation is important because house is exposed to the seasonal and diurnal variations in temperature outside. The plastic foam is occasionally used as the core of a sandwich structure, located between structural panel faces to fashion a structural insulated panel. However, the plastic foams and mineral wools are not advantageous in non-steady-state insulation for house over insulation board, whereas they are suitable for steady-state insulation.

OBJECTIVES The author has speculated that a wood-based sandwich panel with low-density fiberboard can serve as an alternate structural insulated panel. The lightweight fiberboard is required to be a high-performance wood-based insulator with improved mechanical properties for the core use. The wood-based sandwich panel with the low-density fiberboard is considered to have a potential to enable alternative house designs, providing with comfortable environments for human indoor life. The conventional optimization method for sandwich structure [1] must be extended to the sandwich panel with low-density fiberboard core for the optimum designing.

By using steam-injection pressing methods and isocyanate resin adhesives, the author aims to develop wood-based sandwich panels with low-density fiberboard for use as structural insulated walls and floors. Two main focuses are given as follows: the establishment the fundamental technologies to develop wood-based sandwich panels with low-density fiberboard, and the development of thick wood-based sandwich panels with a low-density fiberboard core and structural faces for the applications to structural insulated walls and floors.

CONCLUSIONS The properties of low-density fiberboard could be improved using the isocyanate resin adhesive and steam injection pressing technology. These low-density fiberboards (LDFB) were with good dimensional stability, improved specific mechanical properties, and superior thermal and sound insulation properties [2]. Low-density fiberboard was a promising insulator from sustainable wood resource, providing better warmth-keeping property than commercial insulators. The upgraded properties of low-density fiberboard could be applied to the core material of sandwich panels [3]. The lightweight veneer-faced sandwich (VSW) panels with low-density fiberboard provided with many-functions, such as good dimensional stability, high mechanical properties, and good thermal and sound insulation performance.

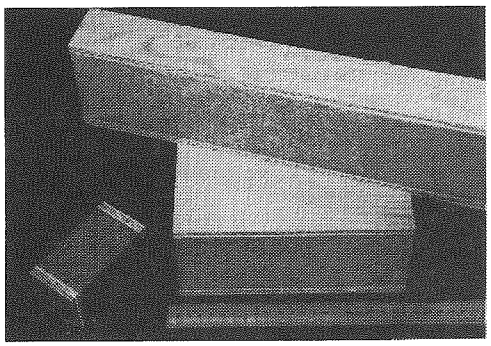

Fig. 1. Samples of plywood-faced sandwich (PSW-T100) panel

These results could be applied to the manufacture of thick wood-based sandwich panels with low-density fiberboard intended for use as structural insulated walls and floors [4]. It was concluded that the plywood-faced sandwich (PSW) panel with a thickness of almost 10 cm (PSW-T100, Fig.1) and with a density of 400 kg/m^3 had the optimum design as a structural insulated wall floor panel among the other several wood-based sandwich panels (Tables 1, 2). Knowledge about the manufacture techniques, the material constants in bending [4] and shearing [5] performance, and the other properties can provide a basis for the practical application of the wood-based sandwich panels to wall/floor panel member in house construction. Its well-balanced

insulation properties [6] will improve the degree of comfort and energy efficiency of our indoor environments and activities in residences exposed to severe temperature changes.

Modern day wood is from species of trees that survived severe climate changes in the history of earth. Because of this, wood will play a greater role in building materials for humans in the future for long. Making most use of the potential of wood, the wood-based sandwich panels with low-density fiberboard were designed and developed for use as structural insulated walls and floors. The required characteristics such as stiffness, appropriate weight and insulation, which could be balanced by the optimized panel products, can ensure sustainable wood as a suitable building material and make contribution to progress the human habitation style in the future.

Table 1. Experimental material constants in four-point bending of the manufactured sandwich panels

No.	Specimen	ρ_{SW} (kg/m^3)	P/δ_L (MN/m)	$E_L I$ ($\times 10^{-6}$ GNm^2)	E_L (GN/m^2)	$E_0 I$ ($\times 10^{-6}$ GNm^2)	E_0 (GN/m^2)	$G_b A$ ($\times 10^{-3}$ GN)	G_b (GN/m^2)	E_L/E_0
1	PSW-T100	320	0.071	4.2	1.2	19	5.1	0.028	0.0060	0.24
2		350	0.18	11	3.0	22	6.2	0.11	0.022	0.48
3		430	0.21	13	3.5	20	5.5	0.18	0.038	0.65
4	PSW-T50	430	0.067	4.0	6.4	5.1	8.1	0.10	0.036	0.79
5		480	0.042	2.5	7.4	2.7	7.8	0.25	0.114	0.95
6	MSW-T100	380	0.086	5.1	1.4	6.5	1.8	0.13	0.026	0.79

ρ_{SW}, density of sandwich panel; P/δ_L, stiffness; $E_L I$, apparent flexural rigidity; E_L, apparent elastic modulus; $E_0 I$, pure flexural rigidity; E_0, pure elastic modulus; $G_b A$, shear rigidity; G_b, shear modulus. The data is average values of the specimens for the bending test. GN/m^2 = GPa = kN/mm^2

Table 2. Optimum design points of the virtual sandwich beams

No.	Face	$\rho_{SW\,opt}$ (kg/m^3)	c_{opt} (m)	f_{opt} (m)	h_{opt} (m)	W_{opt} (kg)	c_{opt}/c	f_{opt}/f	h_{opt}/h	W_{opt}/W
1'	PW	280	0.100	0.0046	0.109	2.29	1.28	0.52	1.14	0.97
2'		340	0.095	0.0077	0.110	2.83	1.23	0.86	1.16	1.08
3'		430	0.082	0.0099	0.102	3.28	1.06	1.10	1.07	1.00
4'		400	0.050	0.0064	0.063	1.89	1.43	0.71	1.18	1.03
5'		450	0.037	0.0060	0.049	1.66	1.43	0.67	1.13	0.99
6'	MDF	390	0.094	0.0098	0.114	3.36	1.22	1.09	1.19	1.20

Optimum core thickness (c_{opt}) and optimum face thickness (f_{opt}) are calculated setting $dW/dc = 0$. From these thicknesses, panel density ($\rho_{SW\,opt}$), panel thickness (h_{opt}), and weight (W_{opt}) at the optimum point are calculated. The results were compared to the data of the manufactured panels in ratios to core thickness (c), face thickness (f), panel thickness (h), and weight (W)

REFERENCES

[1] Gibson LJ, Ashby MF (1997) Cellular solids. Cambridge Univ. Press. Cambridge, pp 345-386
[2] Kawasaki T, Zhang M, Kawai S (1998) *J. Wood Sci.*, 44:354-360
[3] Kawasaki T, Zhang M, Kawai S (1999) *J. Wood Sci.*, 45:291-298
[4] Kawasaki T, Kwang H, Komatsu K, Kawai S (2003) *J. Wood Sci.*, 49:199-209
[5] Kawasaki T, Zhang M, Wang Q, Komatsu K, Kawai S (2006) *J. Wood Sci.*, in printing
[6] Kawasaki T, Kawai S (2004) *J. Wood Sci.*, 52:75-83

Development of wooden semi-rigid frame with improved column and proposal of design methods

Masahiro Noguchi

Structural Engineering Research Center, Tokyo Institute of Technology

Wooden houses are one of the largest utilizations of timbers in Japan. However, in Japan, the life cycles of most houses are around 20-30 years. Recycle ratio of timber as the material resources such as chips and reuses were said around 15 %, including energy resources of around 30 %. This might be considered as the wastes of resources and energies from the global environment perspective. The most governing factor is said that the needs to renewal several equipments and arrangements of rooms can not be met, so-called durability due to the old fashioned uses of the houses, when family organizations and owners change.
As a solution of these problems, open building systems was focused. The open building systems are the building systems that structures were divided into the skeleton parts and the infill parts. Houses were built with the skeleton structures and then owners make the infill such as partition walls and housing equipments and so on. When owners will change, the skeletons allow free partitions of spaces and exchange the housing equipments by future owners. This result in increasing durability of houses.

To develop the skeleton structures, rigid frames whose each node is connected as (semi-) rigid was focused. Because the characteristics of semi-rigid frame structures have following three adaptable characteristics to the skeleton structures, dispensable for shear walls to seismic and wind loads, larger spans to the hinge joints, and adaptable to the present building and structural styles.

Many wooden semi-rigid frame structures now were built, but they always have two problems, too expensive compared with the steel and reinforced concrete structures, and short bays between columns. This is because the shortages of structural performances of wooden semi-rigid frames. Thus, it is necessary to develop semi-rigid frame structures having more effective structural performances.

Moreover, there is another essential problem, the design methods have not been established. Traditional structural styles which have not established structural calculation ways had traditionally changed into the style having structural calculation ways. It was also well-known that the structures designed with structural calculations avoided the big damages under Hanshin-Awaji disaster, although lots of wooden structures without structural calculations were collapsed or damaged a lot. As building and structures are not mass-products, to establish the structural design methods are essential requirements in practice. From above, the key wards of this thesis were set "developments of semi-rigid frame structures with effective structural performances" and "establishing structural design methods of the wooden semi-rigid frame structures".

Firstly, the design methods of knee joints using glued in steel rods (GIR), and cross-lapped glued joints (CLJ) were proposed. In CLJ, I made the hypothesis that both rotational deformation of CLJ and the stress of glue line occurred due to the bending and shear deformation of timber. In GIR, not only the pulling component of rod but also lateral stress component of rod can be taken in account using "theory of the beam on an elastic foundation". From the comparisons between calculations and experimental result, it was recognized that the stiffness and strength in CLJ, and GIR are in good agreement and can therefore be predicted using my models. Therefore, it was thought that the lateral component in the rod has a significant factor for stiffness and strength estimation of GIR. My hypothesis for CLJ can be thought valid within the range of experiments done in this investigation. [1]

In 2nd, a new design method of bolted timber joint was proposed. Considering semi-slip conditions, "moment = 0" and "shear force is equilibrium at the interface between main member and side member, easy formulas for slip modulus and yield strength of bolted timber to timber joint could be derived using "theory of the beam on an elastic foundation". Shear tests having 16 conditions of timber to timber bolted joint whose load angle were varied from 0° to 90° step 30° were performed. From the results, the followings were concluded:

(1) Thinking of 'Semi-slip condition', estimating method of Kuenzi could be simplified.
(2) From results of simulation concerning 15000 combinations, I could derive a kind of closed-form equation to estimate yield load based on TBEF for practical design method. [2]

In 3rd, a new design method of bolted cross lapped joint was developed to estimate the performance of bolted timber joints, in more practical manner, not based on computer simulation. From the theoretical and experimental results, it can be concluded that the rotational stiffness and yield moment in bolted cross-lapped joints can be precisely predicted by using the proposed theory. In the case of rectangular bolt arrangement,

the rotational stiffness calculated using conventional theory is about twice as much as experimental results. Therefore, it is not reasonable to use conventional theory for estimating rotational stiffness in the case of the rectangular arrangement of bolts, but we should use my proposal design method. [3]

Finally, two types of wooden semi-rigid frame structures were proposed. Both structures have improved columns. First type was the structures changed the location of moment resisting ductile joint with improved columns. The second type of structure whose panel zone was extended using improved column. From the test results, the stiffness were improved around 1.7 and 3.5 times as large as that of control, the strength were improved around 1.25 and 1.45 times, respectively. Therefore, the semi-rigid frame structures with improved columns have structural advantages, especially in stiffness. [4]

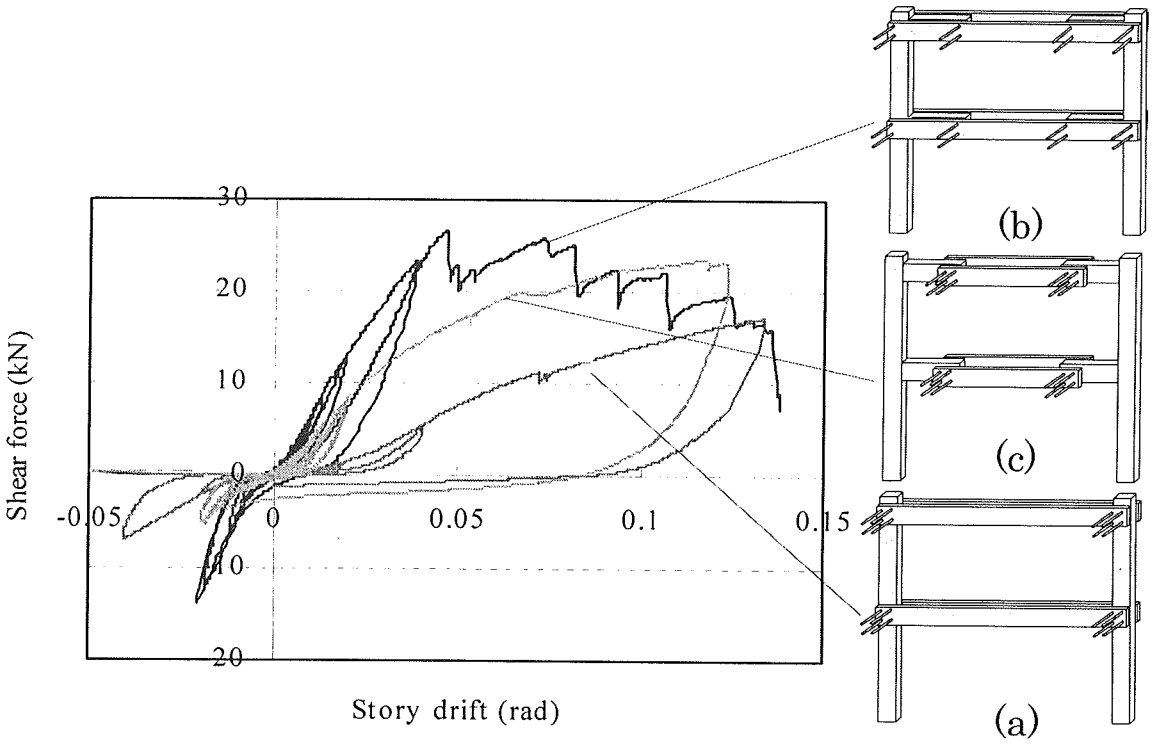

Fig. 1 Shear force-Shear deformation angle relationship
Legend: (a) The structure with traditional bolted cross lapped joints
(b) Proposed structure whose panel zones were extended with the improved column
(c) Proposed structures changed the location of moment transmitting connection with improved columns

In conclusion, this thesis proposes two semi-rigid timber frames with a more effective structural performance are compared and a structural design method is derived. Usually the joints are located at the intersection of the beam and the column. The first frame type applies two types of joints. A high strength capacity rigid glued joint is used to replace the traditional beam-to-column joint while a second ductile semi-rigid joint is positioned at the area with low bending moments.. The beam pieces that run between the column and the semi-rigid joints are so well fixed to the column that they form one integral part. In the second frame type the horizontal beam between the columns is extended beyond the location of the semi-rigid joints of the first frame. This creates a large overlapping area where mechanical fasteners such as bolts are generously spaced. Due to the large fastener spacing the stiffness is enhanced as well as the strength.

REFERENCES

[1] Noguchi, M., Komatsu, K. : J. Wood Sci, *in press*
[2] Noguchi, M., Komatsu, K.(2003) *Mokugaikkaishi*, vol. 49, no. 2, p. 92-103
[3] Noguchi, M., Komatsu, K. (2004) Journal of Wood Science, vol. 50, no. 5, p. 391-399
[4] Noguchi, M., Takino, S., Komatsu, K. (2006) J. Wood Sci, vol. 52, no. 1, p. 51 – 57

Compressive deformation behavior of wood impregnated with low molecular weight phenol formaldehyde (PF) resin

Md. Iftekhar Shams

Laboratory of Active Bio-based Materials, RISH, Kyoto University, Japan

The establishment of a sustainable society based on renewable and sustainable resources is desirable in the twenty-first century. In this sense, wood may be considered as a future-oriented material even though it is one of the oldest materials. However, wood possesses disadvantages like dimensional instability to moisture, low durability due to bio-deterioration and poor mechanical properties compared to other engineering material. To overcome these drawbacks, combination of PF resin impregnation and compression seems to be promising method by which dimensional stability and mechanical properties of wood could be improved considerably. PF resin impregnated compressed wood named as Compreg, exhibited high strength, good dimensional stability and high resistance to decay and termites [1]. However, processing this material is severely curtailed by the need for high hot pressing pressures in order to achieve its highly compressed condition, which results in a high cost product thus having limited applications. Hence, a method to obtain highly compressed wood at low pressing pressure was developed based on the analysis of the deforming behavior of PF resin-impregnated wood.

At first, the deformation behavior of low molecular weight phenol formaldehyde (PF) resin-impregnated wood under compression in the radial direction was investigated [2, 3]. Flat sawn grain Japanese cedar (*Cryptomeria japonica)* block with a density of 0.34 g/cm^3 were treated with aqueous solution of 20 % low molecular weight PF resin resulting in weight gain of 60.8%. Oven dried specimens were compressed using hot plates fixed to a testing machine. The temperature was 150°C and the pressing speed was 5mm/min. The impregnation of PF resin caused significant softening of the cell walls resulting in collapse at lower pressing pressures. With an increase of PF resin content, the Young's modulus of the cell wall perpendicular to the fiber direction decreases, and collapse initiating pressure decreases linearly with the Young's modulus. This indicates that the occurrence of cell wall collapse is strain dependent. Thus, pressure holding causing creep deformation of the cell walls was also effective in initiating cell wall collapse at a lower pressing pressure. Utilizing a combination of low molecular weight PF resin impregnation and pressure holding at 2 MPa resulted in a density increase of PF resin treated wood from 0.45 to 1.1 g/cm^3. Concurrently, the Young's modulus and bending strength increased from 10 GPa to 22 GPa and from 80 MPa to 250 MPa, respectively. It can be concluded that that effective utilization of the collapse region of the cell wall is a desirable method for obtaining high-strength PF resin-impregnated wood at lower pressing pressures.

Considering the application of this technique, the effects of the raw material or species was further clarified [5]. The deformation behavior of resin-impregnated wood up to 10 MPa was significantly different among the species. When PF resin-impregnated wood was compressed up to 2 MPa and the pressure was kept constant for 30 minutes, the density of Japanese cedar reached 1.18 g/cm^3, about 30% higher than the density of compressed Japanese birch, which possesses a 2.5 times higher original density. The mechanical properties of resin-impregnated wood, especially low density wood, increased with density. Hence, it is manifested that low density wood species such as Japanese cedar, albizia have an advantage as raw materials for obtaining high-strength wood at lower pressing pressure.

To obtain a further drastic deformation of PF resin-impregnated wood under compression, the effect of the removal of the matrix substances of the cell wall prior to resin impregnation was studied [4]. $NaClO_2$ treatment has shown considerable potential for high compression of PF resin-impregnated wood at lower pressing pressure, especially after adding moisture of 10-11%. This deformation is further enhanced during pressure holding by creep deformation. The density, Young's modulus and bending strength of four times $NaClO_2$ treated PF resin-impregnated veneer laminated composites compressed at 1 MPa, reached 1.15 g/cm^3, 27 GPa and 280 MPa, whilst those values in untreated PF resin-impregnated wood reached 0.8 g/cm^3, 16 GPa and 165 MPa, respectively.

The above treatment is attractive; nevertheless it is complicated in processing. Furthermore, it is somewhat difficult to remove the harmful chemical, $NaClO_2$, completely from the treated wood, a factor that poses a major drawback in the application of this treatment. Hence, the potential of steam pretreatment as a substitute treatment for making highly compressed PF (phenol formaldehyde) resin-impregnated wood at a low pressing pressure was evaluated [6]. The pressing pressure-density relationship of steam treated resin-impregnated wood is compared in Fig. 1 with those of $NaClO_2$ (a lignin removal treatment) treated

resin-impregnated wood [4]. The weight loss due to $NaClO_2$ treatment was 21%, and the weight gain due to PF resin impregnation for $NaClO_2$ treated wood was 60%. As reported previously [4] there was a significant difference in compressibility between air-dried and oven-dried conditions for $NaClO_2$ treated PF resin-impregnated wood. The density of $NaClO_2$ treated resin-impregnated wood was 0.7 g/cm^3 for the oven-dried condition ($NaClO_2$ treatment, OD) at a pressing pressure of 1 MPa. After adding moisture of 10-11% to the $NaClO_2$ treated resin-impregnated wood ($NaClO_2$ treatment, AD), the density reached 1.0 g/cm^3. This is similar to the density attained by oven-dried steam treated resin-impregnated wood (200°C). It is thus recommended that steam treatment can be substituted for chemical treatment in the fabrication of highly compressed PF resin-impregnated wood, since steam treatment is much easier than the $NaClO_2$ treatment and is harmless to humans.

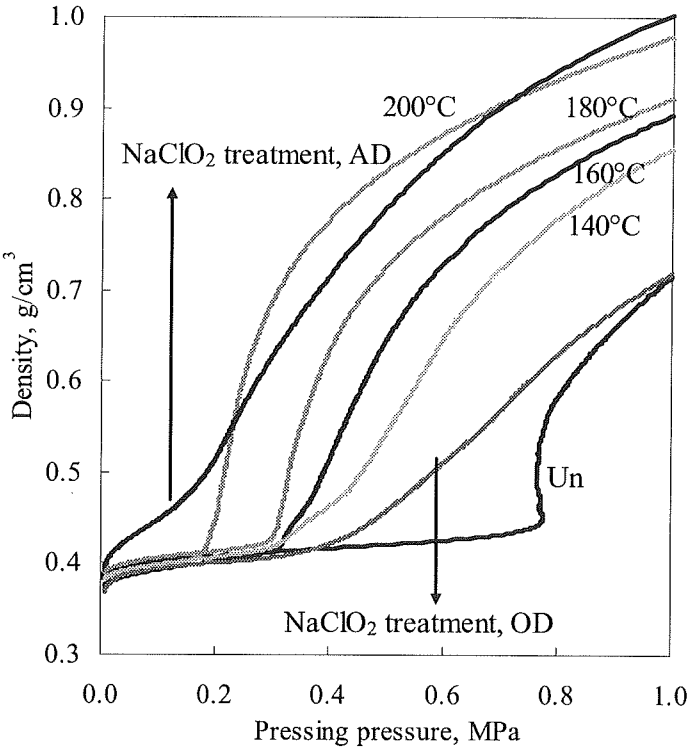

Fig. 1 Changes of density of PF resin-impregnated wood as a function of steaming temperature and comparison with those of $NaClO_2$ treatment [4]. AD and OD refer to air- dried and oven-dried conditions for NaClO2 treated PF resin-impregnated wood, respectively. Un refers to PF resin impregnated wood. Steaming time was 10 minutes

Considering that 1 MPa is a typical pressing pressure used for ordinary plywood and LVL production, our preliminary finding [7] indicates that overlaying veneer plasticized by low molecular weight PF resin on the particle mat before hot pressing resulted in selective densification of surface veneer, and improved the mechanical properties of particleboard significantly with a slight increment in density.

REFERENCES

[1] Stamm AJ (1964) Ronald press, New York, pp 343-358
[2] Shams MI, Yano H, Endou K (2004) J Wood Sci 50: 337-342
[3] Shams MI, Yano H (2004) J Wood Sci 50: 343-350
[4] Shams MI, Yano H, Endou K (2005) J Wood Sci 51: 332-336
[5] Shams MI, Kagemori N, Yano H (2006) J Wood Sci (in press)
[6] Shams MI, Morooka T, Yano H (2006) J Wood Sci (in press)
[7] Shams MI, Yano H, Kawai S (2003) Wood Research 90:17-18

A study on search performance and beam-forming method of multi-beam radar

Shoji Matsuda
Research Institute for Sustainable Humanoshere (RISH), Kyoto University

Multi-beam search-radar systems have been recently developed with the progress in phased-array antennas and digital beam-forming technology [1]. However, the characteristics of multi-beam radar and its optimum design have not been sufficiently studied. In this thesis, a systematic design method for multi-beam search radar which clarifies the relation between radar parameters and theoretical performance is proposed. Beam-forming methods and their performance in new applications to which multi-beam radar technology is indispensable are also discussed.

The first half of this thesis describes a simple model which expresses the relation between radar parameters and search-radar performance for multi-beam radar and proposes an optimum design method to minimize equipment size using a nonlinear optimization technique to satisfy required performance.

Three specific merits of multi-beam radar compared with single-beam radar are described. First, it is theoretically clarified that improvement in Doppler resolution (that is, clutter suppression performance) is obtained without influencing other performances. Second, it becomes possible to apply a radar resource-management technique to control the number of beams and the beamwidths and to adapt to the radar environment. This technique improves in search data rate or clutter suppression. Third, detection performance is improved by using the correlation between signals received in the multiple beams. Here, new correlation methods for multi-beam radar -- Multiple thresholds detector and RMS detector -- are proposed for which the relation between beam spacing and required signal-to-noise ratio (SNR) is determined using numerical simulation.

The latter half of this thesis discusses beam-forming methods and search-radar performance for "bistatic radars" and "distributed-array radars" which is novel applications of multi-beam technology.

For bistatic radar the pulse-chasing technique using a single beam is a beam-forming method established for search-radar [2]. However, the required wider beamwidth and faster beamwidth control have been large obstructions to its utilization. Here the multi-beam pulse-chasing technique [3] using a receiving multi-beam stack is proposed as a means to avoid these problems, and the required number of beams and received SNR are discussed as a function of target position. The numerical examples show that the multi-beam pulse-chasing method achieves several decibels improvement of SNR compared with a single beam (Fig.1(a)). In addition, an improvement that reduces the number of beams (namely reduces necessary signal-processing) is proposed. This method treats a received signal for which a part of the pulse is lacking, as in the case of pulse-compression waveforms. The relation between the SNR loss and the ratio of upper limit and full number of beams is shown based on numerical calculations (Fig.1(b)).

Distributed-array radar [4] is an advanced and attractive concept in which a number of small sub-arrays are synthesized to provide high detection performance. However, the conventional data-independent beam-forming (NB) approach is unsuitable for such distributed sub-arrays because they produce many grating lobes. Therefore, for search-radar mode a novel blind multi-beam forming method that uses an eigenvector corresponding to the maximum eigenvalue of the sub-array-based input correlation matrix is proposed and its performance is investigated with numerical examples. This method provides both an increase in receiving-antenna gain in proportion to the number of sub-arrays and an expansion of the synthesized beamwidth relative to each sub-array's beamwidth, which can provide extreme improvement to search efficiency for distributed-array radars.

In addition, for the acquisition and tracking mode a norm-constrained diagonal-loading Capon beam-forming method (DL+NCCB) is proposed, which can provide a narrow beamwidth for higher spatial resolution. Moreover this approach prevents both the generation of grating lobes and excessive sharpening of the synthesized beam compared with the well-known standard Capon beamformer (SCB) [5], the fixed diagonal loading robust Capon beamformer (DLCB) [6], and the norm-constrained robust Capon beamformer (NCCB) [7] as shown in Fig.2. Then the influence of norm-constrained parameter (ε) and diagonal-loading parameter (ζ) on the grating lobes and beamwidth are investigated, and the relation between the optimum parameters and performance is shown based on numerical calculations.

It is expected that the technology of sensors including radars will evolve into network sensors that consist of distributed sensors and received data fusion based on multi-beam radar technology in order to satisfy various needs in an information society.

The basic performance and design method for multi-beam radar technology are clarified in this thesis, showing the direction of future radar research. Novel applications specific to multi-beam radar are

discussed. Consequently, this study is expected to contribute to the development of research on future radars and related fields.

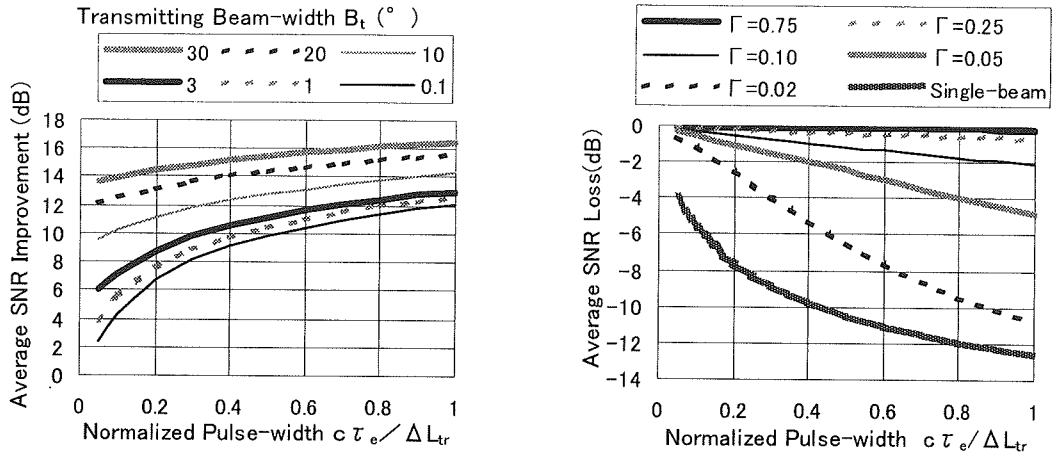

(a) Average SNR improvement of the multi-beam pulse-chasing compared with a single beam (Number of beams is not limitted)

(b) Average SNR loss via the ratio of upper limit and full number of beams Γ at multi-beam pulse-chasing (Transmitting beamwidth Bt=1°)

Fig.1. Received SNR performance of bistatic radar using multi-beam pulse chasing compared with single-beam.

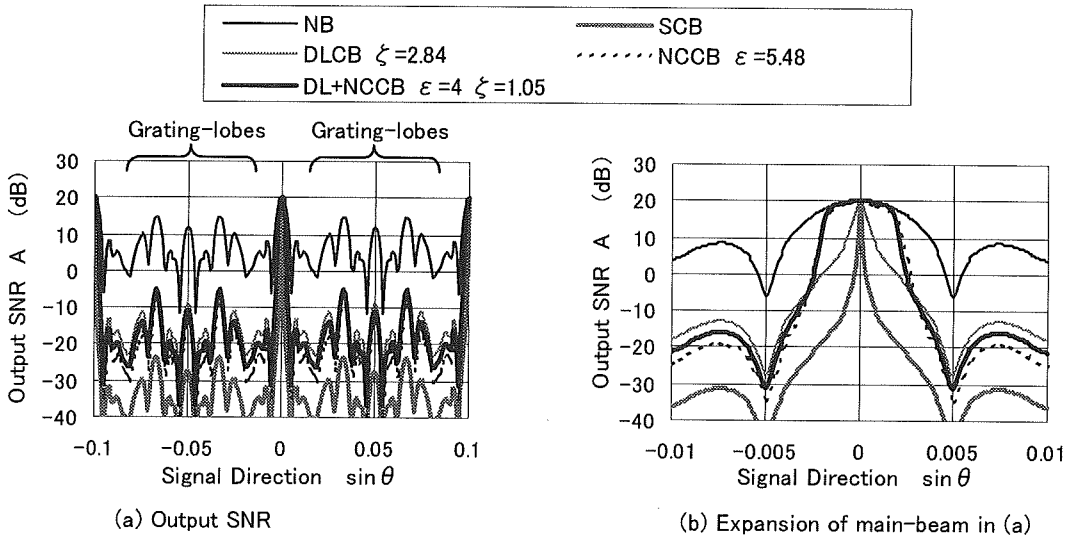

(a) Output SNR

(b) Expansion of main-beam in (a)

Fig.2. Numerical examples of beamformer output of distributed array radar. (Number of subarrays=10 with 30 λ and 40 λ spacing, λ : wavelength)

REFERENCES

[1] Cheston, T. C. and Frank, J. (1990) Radar Handbook Second Edition, McGraw-Hill, New York Chap.7:7.1-7.82

[2] Hanle, E. (1986) IEE Proc, Pt.F, 133(7):587-595

[3] Matsuda, S., Hashiguchi, H. and Fukao, S. (2006) Electronics and Communications in Japan, Part 1, 89(1):11-21

[4] Heimiller, R. C., Belyea, J. E. and Tomlinsonr, P. G. (1983) IEEE Trans. Aerospace and Electronic Systems, 19(6):831-839

[5] Capon, J. (1969) Proc. IEEE, 57(8):1408-1419

[6] Cox, H., Zeskind, R. M. and Owen, M. M. (1987) IEEE Trans. Acoustics, Speech, and Signal Processing, 35(10):1365-1376

[7] Li, J., Stoica, P. and Wang, Z. (2003) IEEE Trans. Signal Processing, 51(7):1702-1715

An observational study of fog structure and dynamics with a millimeter-wave scanning Doppler radar

Akihisa Uematsu
Laboratory of Radar Atmospheric Sciences, RISH, Kyoto University

It is important to obtain mesoscale (~ several kilometers) structure of fog for modeling and forecasting. Recent studies show that fog layer has been observed to have a certain organized structure, such as cellular, roll, or band structure. Other studies show that convective and/or dynamic instabilities, shear instabilities, or gravity waves, have some influences on fog structure and dynamics. Recent advance of remote sensing technology enables us to investigate mesoscale structure and dynamics of fog. Satellites, Lidars, and millimeter-wave radars provide us a fine-scale structure of fog with a resolution of several handled meters or better. Especially, with a millimeter-wave radar, inner structure of fog can be obtained [1]. Kyoto University developed a 35-GHz scanning Doppler radar in collaboration with Mitsubishi Electric Corporation [2]. This radar has 100-kW peak power and 2-m parabolic antenna, hence three-dimensional structure and movement of fogs can be observed. With this radar, observations of sea fog were carried out in Kushiro District, Hokkaido Prefecture in the summer seasons of 1999-2002. Three-dimensional structure of sea fog, vertical and horizontal distributions, and advection were obtained by the radar for the first time.

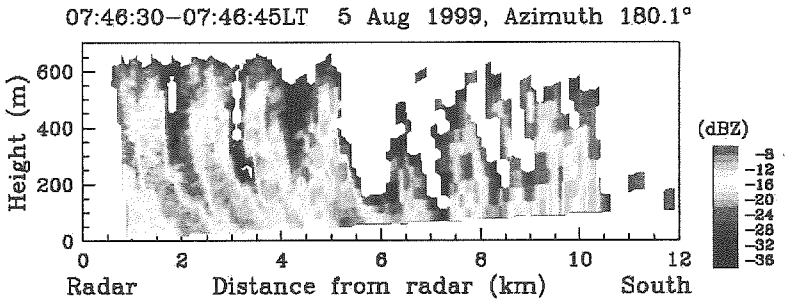

Fig. 1 Vertical cross section of radar reflectivity obtained at 0746 LT on 5 August 1999, shows cellular structure of sea fog.

Fog echo can be classified into the following three typical types: cellular echoes with high radar reflectivity factors (~ −10 dBZ), uniformly distributed echoes with high reflectivities (~ −10 dBZ), and uniformly distributed echoes with low reflectivities (~ −30 dBZ). The two cases of advection fogs with cellular echoes were focused: on 5 August 1999 and 31 July 2000 [3]. Echoes showed structures of cells with a reflectivity of −10 dBZ and with intervals of about 1 km (Fig. 1). This echo pattern moved northward (i.e., from the sea to the land). There was a vertical shear of the horizontal wind at a height around 200 m in both cases, and structures of each cell were upright above the shear line, and leaning below it. The direction and the speed of the echo pattern in both PPI and RHI display agreed well with that of the horizontal wind at heights above the

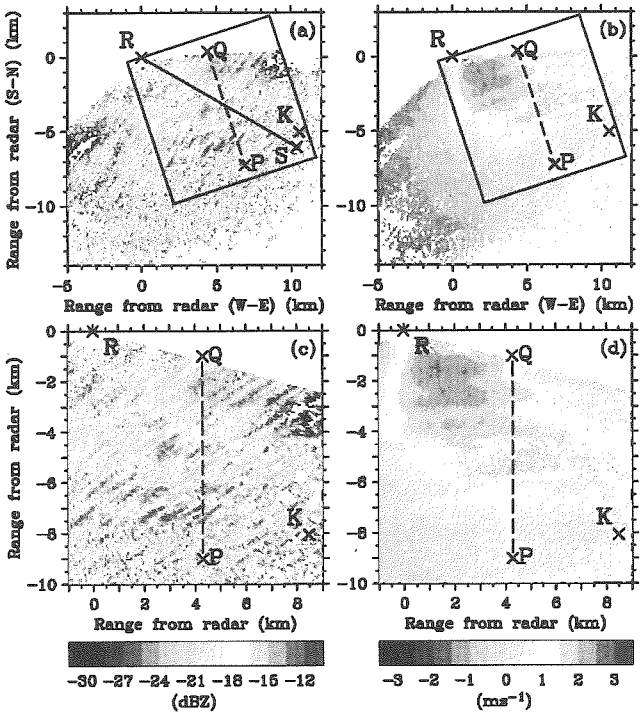

Fig. 2 Horizontal distribution of (a) Radar reflectivity and (b) Doppler velocity obtained at 0129 LT on 1 August 2000. (c) and (d) Extracted data shown in the squares of (a) and (b). This figure shows existence of roll structure (~ 300-400 m scale) in radar reflectivity, and band structure (1.5 km scale) in both radar reflectivity and Doppler velocity.

shear (200 m). These results implies that existence of drizzle drops is implied in the echo cell, and the fog droplets or the drizzle drops with certain falling speeds are being seeded from above.

Three-dimensional roll structure of fog induced by Kelvin-Helmholtz instability (KHI) was presented for the first time [4]. The case of fog with a roll structure observed on 1 August 2000 was analyzed with a millimeter-wave scanning Doppler radar and a rawinsonde data. Roll structure in a fog layer with a horizontal scale of ~ 300-400 m was observed (Fig. 2 (a) and (c)). When the roll structure was observed, extremely large vertical shear (exceeding 50 m s^{-1} km^{-1}) existed below 120 m altitude. The direction of the shear was perpendicular to the roll direction. The Richardson number was less than 0.25 at the shear altitude. This indicates that the fog roll structure was induced by KHI.

Band structure of fog associated with gravity waves was shown for the first time [5]. Band structure in fog having radar reflectivity > −21 dBZ and a scale of ~ 1.5 km was observed (Fig. 2 (a) and (c)). The band structure was also observed in Doppler velocity (Fig. 2(b) and (d)). The band structure in both radar reflectivity and Doppler velocity propagated northwestward with a speed of 4.17 m s^{-1} (Fig. 3). From linear gravity-wave theory it is estimated that the observed gravity waves had a horizontal wavelength of 1.5 km and period of 6 min.

Within the band structure induced by the gravity waves (horizontal scale ~ 1.5 km), roll structure with a smaller horizontal scale (~ 300-400 m) was also observed in radar reflectivity. A previous study has shown that this smaller-scale roll structure is caused by shear-induced KHI. For the first time this study shows that two factors, gravity waves and KHI, can cause multi-scale structure in fog.

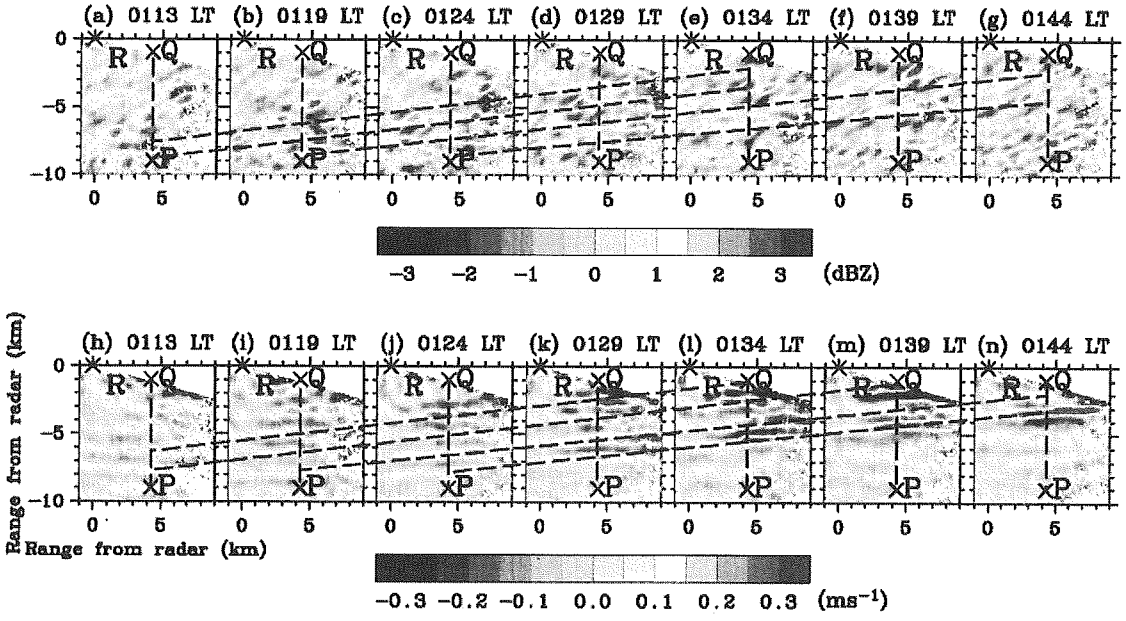

Fig. 3 (a)-(g) Radar reflectivity and (h)-(n) Doppler velocity fluctuations obtained at every 5 minutes at 0113-0144 LT on 1 August 2000, shows structure and propagation of band structure (1.5 km scale).

REFERENCES

[1] Yanagisawa, Z., M. Ishihara, and T. Sawai (1986), Tenki, 33:603-612 (in Japanese).
[2] Hamazu, K., H. Hashiguchi, T. Wakayama, T. Matsuda, R. J. Doviak, and S. Fukao (2003), J. Atmos. Oceanic Technol., 20:972-986.
[3] Uematsu, A., H. Hashiguchi, M. Teshiba, H. Tanaka, K. Hirashima, and S. Fukao (2005a), J. Appl. Meteor., 44:1260-1273.
[4] Uematsu, A., M. K. Yamamoto, H. Hashiguchi, K. Hirashima, and S. Fukao (2005b), Geophys. Res. Lett., 32, L14824, doi:2005GL022423.
[5] Uematsu, A., H. Hashiguchi, M. K. Yamamoto, S. K. Dhaka, and S. Fukao (2006), J. Geophys. Res., in revision.

Expression and structure-function analysis of a versatile peroxidase

Ryota Sakai
Laboratory of Biomass Conversion, RISH, Kyoto University

INTRODUCTION

White rot fungi are a family of basidiomycetes and degrade plant cell wall lignin. They produced ligninolytic enzymes, laccase (Lac), lignin peroxidase (LiP), manganese peroxidase (MnP) and versatile peroxidase (VP). VP is produced by *Pleurotus* and *Bjerkandera* species [1,2] and has enzyme properties of both MnP and LiP, namely, oxidation of Mn^{2+} and high redox-potential aromatic compounds. Moreover, *P. ostreatus* MnP2, one of the VPs, can even oxidize directly high molecular-weight substrates such as RNase A and Poly R-478 [3]. In contrast, *Phanerochaete chrysosporium* LiP H8, a typical LiP, oxidizes directly veratryl alcohol (VA) at an exposed tryptophane residue (W171), however, it required appropriate mediators to oxidize high molecular-weight substrates with high redox potential. In MnP2, W170 was suggested to be the redox active site for VA, RNase A and Poly R-478 by a chemical modification of the enzyme [3].

In this study, we expressed four mutants of MnP2 (W170A, R263N, Q266F and V166/168L) using a homologous expression system and structure-function analyses were done.

MATERIALS and METHODS

Wild type (WT) and four mutants were expressed in *P. ostreatus* homologous expression system [4] and purified from the culture fluid. Purified proteins were analyzed in view of isoelectric point and molecular weight using IEF and SDS-PEGE. WT and four mutants were measured catalytic activity for low molecular-weight substrates (Mn^{2+}, H_2O_2 and VA) and K_m and V_{max} values were determined. Oxidizing activity for high molecular-weight substrate was evaluated by dimerization activity of RNase A (13.7 kDa).

RESULTS and DISCUSSION

Except for R263N, the molecular weight and isoelectric point of the mutants were the same as those of WT. While, possibly caused by a new N-glycosylation site was added, the molecular weight and isoelectric point were slightly different in R263N.

W170A was demonstrated to lose oxidizing activity for VA but the other low molecular-weight substrates was oxidized as did WT. Catalytic activity of Q266F and V166/168L was decreased only for high molecular-weight substrate RNase A. Comparing of a three-dimensional structure model of the two mutants (Q266F and V166/168L) with that of WT and LiP H8, there were steric hindrances around W170 of the mutants, which are similar to LiP H8. Therefore, we concluded that, in wild-type *P. ostreatus* MnP2, high molecular-weight substrates can access W170 where one electron is abstracted *via* long length electron transfer pathway, and that the access was blocked by the surrounding steric hindrances in Q266F, V166/168L and *Ph. chrysosporium* LiP H8.

REFERENCE

[1] Martinéz MJ, Ruiz-Dueñas FJ, Guillen F, Martinéz AT. (1996) Eur J Biochem, 237(2):424-32.
[2] Mester T, Field JA. (1998) J Biol Chem, 273: 15412-15417.
[3] Kamitsuji H, Watanabe T, Honda Y, Kuwahara M. (2005) Biochem J, 386(Pt 2): 387-93.
[4] Tsukihara T, Honda Y, Watanabe T, Watanabe T. (2005) Appl. Microbiol. Biotechnol, on line publication, DOI:10.1007/s00253-005-0136-1

Development of a novel transformation system in basidiomycetes

Naofumi Sakatoku
Laboratory of Biomass Conversion, RISH, Kyoto University

White rot fungi are known to degrade plant cell lignin and also various aromatic pollutants. Intensive research has been done to make use of their special function for a novel carbon recycle system and also bioremediation of polluted environments, which will contribute for development of a sustainable society. Especially, a selective white rot basidiomycete, *Ceriporiopsis subvermispora* is a promising microorganism which is effective as a biocatalyst to degrade lignin in industrial processes, including pulp and paper manufacture, and conversion of lignocellulosic biomass to various compounds. However, there is no report on development of a transformation system in this fungus. Transformation techniques are valuable tools for not only molecular biological analysis of the selective lignin degradation system but also strain improvement of desired phenotype.

Transforming vector plasmids were designed to contain bialaphos resistant marker gene (*bar*), from *Streptomyces hygroscopicus,* under control of homologous *gpd* promorter and terminator. In pCsG-*bar*, promoter was fused directly with the cording sequence of *bar* gene, whereas in pCsGi-*bar*, the promoter and the first intron of *gpd* gene were inserted at the 5′end of the cording sequence of *bar* gene, since Ma *et al.* reported that an intron insertion enhanced GFP expression [1].

In this research, we tried to develop a transformation system for basidiomycete *C. subvermispora* using the recombinant plasmids including pCsG-*bar* and pCsGi-*bar* by PEG/$CaCl_2$ protcol and particle bombardment. Moreover, as a control, transformation of *Pleurotus ostreatus* by particle bombardment was performed.

REFERENCE

[1] Ma B., Mayfeield M.B. and Gold M. H. (2001) Appl. Environ. Biotechnol. 67(2): 948-955

Treatment of the fermentation inhibitors from wood by *Trametes versicolor* RC3 Laccase

Keisuke Nishi
Laboratory of Biomass Conversion, RISH, Kyoto University

INTORODUCTION

For an efficient ethanol production from wood biomass resources, a pretreatment step is essential to remove lignin which covers cellulose in the plant cell wall. Ethanolysis is one of the proposed pretreatment steps and separates wood into a pulp fraction and soluble fraction (SF). We have demonstrated that the SF contains furfural, vanillin, syringaldehyde, 5-hydroxymethylfurfural (5-HMF), 3-methyl-2,5-furandion, levulinic acid which are produced in the pretreatment step and that they inhibit the following fermentation to produce ethanol [1]. To obtain high yield of the ethanol production from wood biomass, it is necessary to minimize the influences of these wood-originated fermentation inhibitors produced in the pretreatment process. We founded that a white rot fungus *Trametes versicolor* RC3, which was isolated from Thailand [2], secreted laccase isozymes and they abolished the inhibitory effect of the compounds and promoted the fermentation efficiency of the SF by *Pichia stipitis*[3]. In the present study, to elucidate the removal mechanism of fermentation inhibitors by *T. versicolor* RC3 laccase, we conducted gene cloning and heterologous expression of a RC3 laccase isozyme and analyses of the reaction products of the fermentation inhibitors treated by *T. versicolor* RC3 laccase fractions using GC-MS.

MATERIALS and METHODS

We purified a laccase isozyme with pI value 8.35, using the gel filtration and ion-exchange chromatography and the N-terminal amino acid sequence was determined. Using degenerated primers for the gene encoding this isozyme, a DNA fragement was amplified by PCR and cloned. After cloning of the flunking sequences, we constructed an expression plasmid which has *P. ostreatus sdi1* promoter followed by the coding sequence of the cloned laccase gene from *T. versicolor* RC3. The expression plasmid was introduced in *P. ostreatus* and extracellular laccases were characterized. On the other hand, 5-HMF, vanillin, syringaldehyde and the SF was treated with the acidic or alkaline fractions of laccase from culture filtrate of *T. versicolor* RC3, at 45°C for 24 hour, and the resulting compounds were analyzed by GC-MS.

RESULTS and DISCUSSION

The determined nucleotide sequence demonstrated that the cloned gene encodes a new laccase isozyme, but not isozyme of pI 8.35, and the recombinant gene was expressed to produce an isozyme of pI 2.94 in *P. ostreatus*. We also found that acidic fraction of *T. versiclor* RC3 laccases degraded 5-HMF, vanillin, syringaldehyde as well as, or better than, the other laccases from the same strain. Moreover, it was demonstrated that the acidic fraction was significantly stable against incubation with SF compared to any other laccases tried, suggesting possible contribution of this fraction in the high removing activity of fermentation inhibitors by RC3 laccases.

REFERENCES

[1] Nakamoto H. (2005) Div. Appl. Life Sci., Graduate School of Agric Sci., Kyoto Univ., Master thesis.
[2] Khanongnuch, C. et al. (2004) Fungal Diversity, 15, 187-196
[3] Wada M. (2004) Div. Appl. Life Sci., Graduate School of Agric Sci., Kyoto Univ., Master thesis.

Lipid metabolites produced by the selective white rot fungus, *Ceriporiopsis subvermispora*

Yuko Kawasaki
Laboratory of Biomass Conversion, RISH, Kyoto University

Wood biomass, which is a noteworthy resource for recyclable and substitute petroleum, includes polysaccharides (cellulose and hemicellulose) and lignin. For making use of wood biomass as resources, delignification is necessary. A selective lignin-degrading basidiomycete, *Ceriporiopsis subvermispora* is able to degrade lignin in wood without intensive damage of cellulose. During wood decay by this fungus, extensive delignification was observed without penetration of extracellular enzymes into wood cell wall regions [1]. This indicates that *C. subvermispora* has unknown delignification systems catalyzed by low molecular weight metabolites. We demonstrated that *C. subvermispora* produced saturated and unsatulated free fatty acids during the early stage of wood decay. We also isolated a series of novel alk(en)ylitaconates (ceriporic acids) that inhibit cellulose degradation by the Fenton reaction [2, 3]. The objective of this study is to elucidate correlation between fatty acid metabolism and alk(en)ylitaconate biosynthesis. Production of lipid-related metabolites and transcription of fatty acid desaturases (FAD) were investigated.

C. subvermispora was cultured in a liquid medium at 28°C for 1 month. Intracellular and extracellular metabolites were extracted with methanol and methanol/chloroform (1:2) for the metabolite analysis, respectively. Extracts were analyzed by gas chromatography/mass spectrometry (GC-MS) and liquid chromatography/electrospray ionization mass spectrometry (LC-ESI-MS). Transcription of FAD was investigated by reverse-transcription polymerase chain reaction (RT-PCR).

In the present study, linoleic acid production and transcription of Δ9-fatty acid desaturase were increased at an early stage of cultivation, while alkenylitaconate (ceriporic acid C) production was increased after 1 week. These results suggest that the cloned FAD gene was not involved in the ceriporic acid desaturation.

REFERENCES

[1] Messener, K. and Srebotnik, E. (1994) FEMS Microbiol. Rev., 13:351-364.
[2] Amirta, R., Fujimori, T., Shirai, N., Honda, Y., and Watanabe, T. (2003) Chem. Phys. Lipid., 126:121-131.
[3] Watanabe, T., Teranishi, H., Honda, Y., and Kuwahara, M. (2002) Biochem. Biophys. Res. Commun., 297:918-923

Cloning of Fatty Acid Desaturase Genes from White-Rot Fungi

Saeko Tsuda
Laboratory of Biomass Conversion, RISH, Kyoto University

A selective lignin-degrading fungus, *Ceriporiopsis subvermispora* is able to degrade lignin selectively without intensive damage of cellulose. This fungus produces large amounts of unsaturated and saturated fatty acids such as linoleic acid (18:2n-6) and palmitic acid (16:0) at an early stage of wood decay, and oxidizes them to produce free radicals and TBARS [1,2]. In addition, *C. subvermispora* suppresses ion redox reactions by producing new fungal metabolites (ceriporic acids A, B, and C), resulting in the inhibition of the production of a cellulolytic active oxygen species (hydroxyl radical: $^{\bullet}$OH) [3-5]. Especially, ceriporic acid C contains a carbon-carbon double bond; hence, it may be synthesized from oleic acid (18:1n-9) which contains a double bond at the C9 position. These observations suggest that unsaturated fatty acids (UFAs) might act as a precursor of various low molecular mass compounds involved in a key reaction of the selective lignin degradation, such as lipid peroxidation. In the biosynthesis of UFAs, fatty acid desaturases are key enzymes that are responsible for the insertion of double bonds into alkyl chains. These enzymes are almost universally found in microbial, plant, and animal cells, where they play important roles in a wide range of physiological processes. However, the molecular relationship between the biosynthesis of UFAs and the lignin degradation in white rot fungi is still remained to elucidate. In this study, we focused on UFAs and related metabolites produced by white rot fungi, and tried to clone fatty acid desaturase genes from a well-known white-rot fungus, *Phanerochaete chrysosporium*, as well as a selective lignin-degrader, *C. subvermispora*.

REFERENCES

[1] Enoki, M., Watanabe, T., Nakagame, S., Koller, K., Messner, K., Honda, Y., and Kuwahara, M. (1999) *FEMS Microbiol. Lett.* **180,** 205-211.
[2] Watanabe, T., Katayama, S., Enoki, M., Honda, Y., and Kuwahara, M. (2000) *Eur. J. Biochem.* **267,** 4222-4231.
[3] Enoki, M., Honda, Y., Kuwahara, M. and Watanabe, T. (2002) *Chem. Phys. Lipids*, **120,** 9-20.
[4] Watanabe, T., Teranishi, H., Honda, Y., and Kuwahara, M. (2002) *Biochem. Biophys. Res. Commun.* **297,** 918-923.
[5] Amirta, R., Fujimori, K., Shirai, N., Honda, Y. and Watanabe, T. (2003) *Chem. Phys. Lipids* **126,** 121-131.

Enzymatic saccharification of Japanese cedar wood by combined pretreatments using a newly isolated white rot fungus and solvolysis

Yasunori Baba
Laboratory of Biomass Conversion, RISH, Kyoto University

The production of ethanol from lignocellulosics has received much attention due to immense potential for conversion of renewable biomaterials into biofuels and chemicals. Since lignin makes the access of cellulolytic enzymes to cellulose difficult, it is necessary to decompose the network of lignin prior to the enzymatic hydrolysis. Japanese cedar (*Cryptomeria japonica*) shares over 60% of forest plantation in Japan. However, it was difficult to obtain sufficient enzymatic saccharification yields from the softwood after conventional thermal pretreatments like microwave irradiation, steaming and steam explosion without the use of strong acids or toxic chemicals. Therefore, we studied a new process using treatments with white rot fungi and solvolysis. When the fungal treatment with *Ceriporiopsis subvermispora* was combined with solvolysis, saccharification yields of Japanese cedar wood increased 7 times than those without the fungal treatment. In addition, we found that a newly isolated white rot fungus was more effective than the biopulping fungus, *C. subvermispora*. The high pretreatment effects with the new strain were found when microwave solvolysis was used, instead of conventional solvolysis in an autoclave.

Efficient Biogas Production by Termites and Their Symbiotic Microorganisms

Seima Kawaguchi
Laboratory of Innovative Humano-Habitability, RISH, Kyoto University

In search of a nonconventional sources of energy and lack of fossil fuels, the relevance of hydrogen as an alternative energy source is increasing day by day. Hydrogen is considered as pollution free fuel for the future. Chemical route of hydrogen production is an energy intensive process, in contrast, the fermentation process is an energy saving with obvious advantages. Methane is also a potential biogas, and is produced by the fermentation of various organic materials. Many trials have been carried out to supply methane to the local community as a part of "Zero-Emission Processing" of bio-waste materials.

To construct the effective energy gas production system with wood-feeding pest termites, effects of diets and antibiotics treatments on hydrogen and methane emissions of workers of the termite, *Coptoterrmes formosanus* Shiraki were investigated as well as the isolation of hydrogen-producing facultative anaerobic bacteria from the termite.

When workers of *C. formosanus* were forced to feed on sapwood powder of Japanese red pine (*Pinus densiflora* Sieb. Et Zucc.), cellulose powder, microcrystalline cellulose, carboxymethyl cellulose (CMC), cellobiose and glucose, the highest emission rate (3.46 nmol/termite/h) was obtained in cellulose powder-fed workers. This was 2.7 times higher than that in wood powder-fed workers. But the dietary effect was not obvious in the methane emission.

Five antibiotics effectively enhanced the hydrogen emission of workers, resulting in the maximum emission rate of 17.5 nmol/termite/h when untreated workers emitted it at the rate of 3.73 nmol/termite/h. Similar to the dietary effect, no special effectiveness of antibiotics treatments was observed on methane emission. These results indicated that protists were the major agents to produce hydrogen in the hindgut of workers of *C. formosanus*, not bacteria, and that the artificial modification of the hindgut microorganisms could be applicable to the energy gas production system with termites.

The hydrogen-producing facultative anaerobic bacteria was isolated from the static culture of the homogenate of workers of *C. formosanus*. They effectively converted glucose to hydrogen in an anaerobic condition. But they were not able to convert wood powder and cellulose to hydrogen. The gene analysis of 16S rRNA of the bacteria showed the 100 % similarity to *Enterobacter cloacae*.

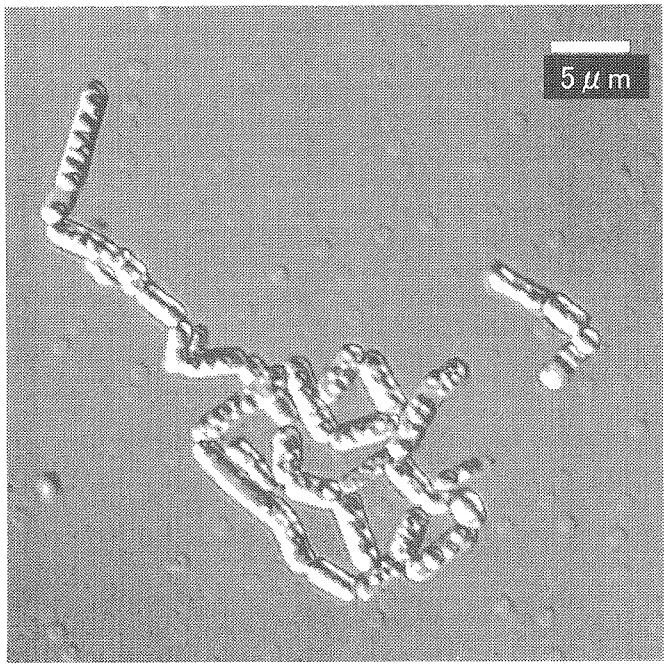

Fig.1. An isolated bacteria from the homogenate of workers of *Coptotermes formosanus*.

Mechanical properties of wood pulp/Poly Lactic Acid green-nano composites

Atsuhiro Iwatake
Laboratory of Sustainable Resources, RISH, Kyoto University

Introduction

Recently 'green-composites' have been focused on materials made from plant fibers and bio-based resins. Plant fibers are not only renewable but also have low density and high strength when compared to glass fibers, which are in common use for making FRP (Fiber Reinforced Plastics). Hence, nano-sized plant fibers are recognized as a potential reinforcing material. Fibrillation of wood pulp fibers is one of the ways to obtain nano-sized plant fibers. There are many reports describing that mechanical and thermal properties of composites are highly enhanced by utilizing such plant nanofibers as reinforcing material. However, most of these nanocomposites were made by special methods, such as film casting, not by melt mixing process, which is quite common in the plastics industry. Melt mixing can be used for general purposes, therefore in this study we applied this method to produce nanocomposites reinforced with plant nanofibers.

The main purpose of this research is to obtain fibrillated wood pulp/PLA nanocomposites by the melt-mixing method and to estimate the influence of degree of fibrillation of wood pulp on the mechanical and thermal properties of the composites.

Materials and Method

Soft wood kraft pulp (PULP), the same pulp treated by 8 passes through a refiner (8 passes refiner PULP), and pulp treated by 30 passes through a refiner and additional passes through a high-pressure homogenizer (Micro Fibrillated Cellulose, MFC) were used as fillers. PLA (LACEA H-280,Mitsui Chemical) was used as the matrix. As shown in Fig. 1, the degree of fibrillation decreases as MFC >8 passes refiner PULP >PULP. These materials were pre-mixed in PLA dissolved in acetone, and after the mixture was dried, melt mixing was performed on a Laboplasto-Mill with a twin rotary roller mixer (Toyo Seiki). The mixing was carried out for 12.5 min at a rotary speed of 40 rpm at 140°C. The compound was pressed into a square shape at 160°C. Specimens were cut from this board into 5 mm (width), 40 mm (length), and 0.3 mm (thickness) pieces. Tensile test of the composites was performed with an Instron 3365 and dynamic viscoelastic measurements was obtained with a Rheovibron (Orientec). The dispersion of fibers and the fracture surface of the composites were observed through an optical microscope and a Scanning Electronic Microscope (JEOL6700F).

Results and Discussion

By premixing filler and matrix in the solvent, we could make well dispersed fiber composites and improve strength and Young's modulus of the composites over the neat PLA. Without premixing, fiber aggregation was formed in the composites and it became more brittle than neat PLA. This premixing is effective for preventing fiber aggregation and making well fiber dispersed composites.

Young's modulus and strength of the composites containing 5wt% MFC were increased almost 20 wt% compared to those of neat PLA, and yield strain was almost the same as that of neat PLA. Otherwise, the composite containing 5wt% PULP had lower strength and also less yield elongation, and became more brittle than neat PLA.

From the results of thermal analysis, it was found that fibrillation of PULP improved the filler-matrix interaction. Thus, we could surmise that fibrillation of PULP enlarged the contact surface area between fibers and PLA, then mechanical properties were enhanced.

Furthermore, we aimed a better improvement of the mechanical properties of the composite, increasing the fiber content of MFC up to 20wt%. As a result, Young's modulus and strength of 10wt% MFC composites were increased 1.4 fold and 1.3 fold respectively. However, strength and yield elongation of composites containing more than 15wt% of MFC were decreased. We conjecture that it was because of fiber aggregation.

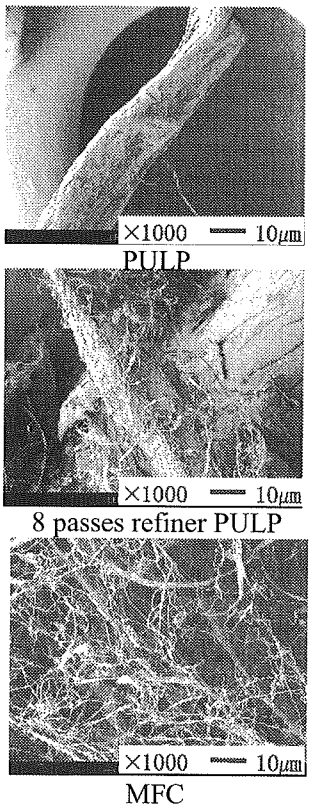

Fig.1 Shapes of each filler

Evaluation of sodium alginate as a wood adhesive

Takashi Okumura
Laboratory of Sustainable Materials, RISH, Kyoto University

INTRODUCTION

Recently, it has been indicated that fossil-based adhesives have serious problems for human health and environment. Natural adhesives derived from non-fossil resources are considered as the alternatives to solve the problems. However, the use of conventional natural adhesives is currently limited because of low bonding properties, especially low water resistance. In addition, conventional natural adhesives need to add some harmful chemical agents for high bonding strength and durability. Therefore, it is extremely important to develop safe natural adhesives with good bonding properties.

Although sodium alginate (SA) is water-soluble natural polysaccharide derived mainly brown seaweeds, water-insoluble property is developed by adding multivalent cations. In this study, the SA was evaluated as a new natural wood adhesive.

MATERIALS and METHODS

The molecular weight and manuronic acid/gulironic acid (M/G) ratio of SA (Kimica-algin IL-2) produced by Kimica Corporation. were 102,000 and 0.71, respectively. Calcium chloride ($CaCl_2$), calcium carbonate ($CaCO_3$) and borax were used as a gelling agent. Plywood was manufactured using rotary-peeled lauan veneer of 1.6mm thickness and the SA as an adhesive. The 3-ply plywoods coated with the SA of 8-48 g/m^2 solid spread rate were hot-pressed at 130°C under 1MPa for 15minutes. Particles were prepared using recycled chips. The SA was added with a solid content of 10%, and the target densities of the boards were 0.4, 0.6, and 0.8 g/cm^3. The particle mats were hot-pressed at 125°C for 40 minutes, and then immersed in 10wt% $CaCl_2$ solution for 5 - 15 min. Finally, the mats were dried at 125°C for 45 - 90 min. The physical properties of plywoods and particleboards bonded with SA were evaluated by JIS K 6851 and JIS A 5908, respectively.

RESTLTS and DISCUSSION

Fig.1 shows the dry bond strength of 3-ply plywood glued with various amounts of SA alone. The bond strength increased with increasing SA to 32g/m^2 and then decreased slightly. In case of the addition of gelation materials, the bond strength was not improved. The water resistance of SA was extremely low.

Fig.2 shows the thickness swelling (TS) of the particleboard. The good dimensional stability was observed in the particleboard with the density of 0.4 and 0.6 g/cm^3, but the remarkable swelling was recognized in the particleboard with the density of 0.8g/cm^3. The value of the internal bond strength of the board of 0.8 g/cm^3 was worst. It seemed that the gelled SA was collapsed partially by the drying process after $CaCl_2$ solution immersion. The results indicated that careful consideration must be given to the gelation mechanisms when using SA as a wood adhesive.

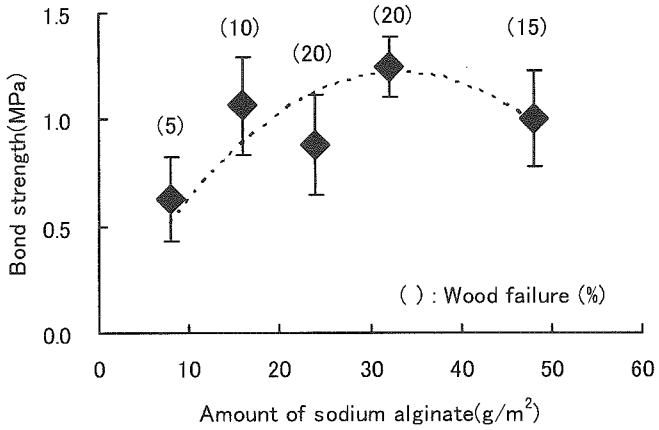

Fig.1 The relationship between SA spread rate and bond strength.

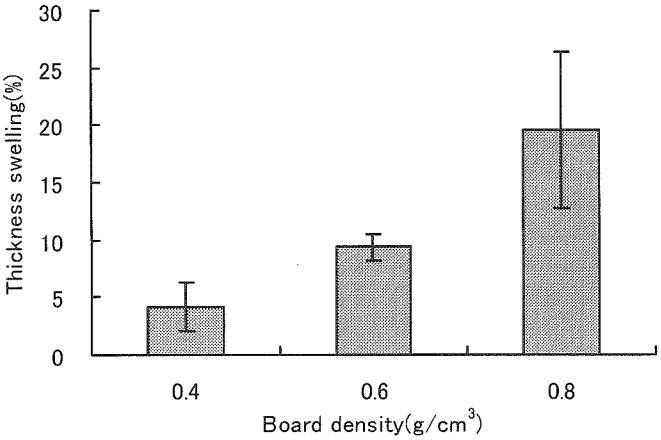

Fig.2 The relationship between TS and board density.

Characterization of plant orthologue of *ABCA1* in *Arabidopsis thaliana*

Masafumi Hamamoto
Laboratory of Plant Gene Expression, RISH, Kyoto University

ATP-binding cassette (ABC) proteins constitute a large superfamily, which occur all organisms inverstigated to date ranging from bacteria to human. In plant, cloning of ABC proteins were reported time to time, and *Arabidopsis thaliana* research has revealed that plants are a big resourse of this protein family, i.e. *Arabidopsis* genome contains a total of ca. 120 open reading frames (ORFs) that encode ABC proteins, which are more than doubleof human ones. AtABCA1 of *Arabidopsis*, the counterpart of human ABCA1 functioning as a regulator of cellular cholesterol homeostasis, is a single copy gene in the genome, whereas its orthologue is not found in yeast and even in rice. This occurrence of hull size ABCA1 suggests that AtABCA1 has physiological functions specific to dicots, or other half size members of ABCA memberes may complement the roles of ABCA1 in rice.

In this study we isolated full-length *AtABCA1* cDNA and carried out the detailed expression analysis of AtABCA1 gene in *Arabidopsis*. Northern analysis of *AtABCA1* in *Arabidopsis* revealed that *AtABCA1* was expressed in all organs, especially higher expression was observed in the stem and the root than leaves. GUS plant analysis showed that AtABCA1 was only expressed in the vascular tissues of root, stem, and leaf through out the growth stage from seedling to adult plant. These results suggest that AtABCA1 is involved in the long-distance transport of endogenous substances. In addition, strong expression was also observed in mature pollen. We determined the subcellular localization of AtABCA1 by use of GFP-fusion prote that was stably expressed in *Arabidopsis* transformant.

When the response of *AtABCA1* gene expression to various plant hormone and related compounds was analyzed with northern blot, its mRNA level increased by abscisic acid treatment, whereas auxin and cytokinin as well as gibberellin did not storongly influence the gene expression. The positive response to abscisic acid was further analyzed in the time course expreriment to show that the expression sharply induced in half a day and was kept at high level up to 7 days. Further investigation on the phenotype analysis under various stress conditions has been done.

Expression analyses and characterization of isoprene synthase from *Populus alba*

Kanako Sasaki
Laboratory of Plant Gene Expression, RISH, Kyoto University

INTRODUCTION

Isoprene is a volatile C5 terpenoid that is released mainly from the leaves of many deciduous broad-leaved trees, such as *Salix*, *Quercus* and *Populus* species. The annual global emission of isoprene from these trees is estimated to be as high as 5 x 10^{14} g of carbon, which is similar to the level of methane, the most abundant naturally emitted hydrocarbon. Isoprene has been suggested to potentially provide general protection against environmental stress, such as heat and water as well as to protect against singlet oxygen.

To obtain biochemical and molecular biological insights into isoprene synthase, we cloned isoprene synthase cDNA from *P. alba* (PaIspS) and studied gene expression in response to environmental stress. Moreover, we examined the subcellular localization of PaIspS and also characterized its enzymatic function with a recombinant protein.

MATERIALS and METHODS

For the expression analyses of *PaIspS*, total RNA prepared from leaves, stems and roots were subjected to semi-quantitative RT-PCR. Expression level of the *PaIspS* was normalized by the *actin* values.

To analyze the subcellular localization of PaIspS, the nucleotide sequence for the putative transit peptide of PaIspS was subcloned into psmRS-GFP (accession number U70496) with a CaMV35S promoter. Onion peels and 1-month-old tobacco leaves were bombarded using a particle gun PDS-1000 according to the manufacturer's instructions. After 24 hr, GFP fluorescence of onion and tobacco cells was observed under a laser scanning confocal microscope.

To quantify the enzymatic activity of PaIspS, the sequence for the putative mature polypeptide of PaIspS was subcloned into pET22b and expressed in *Escherichia coli* origami B (DE3) with isopropyl β-D-thiogalactoside. Crude enzyme, which was prepared by sonication, was used for enzyme assay.

RESULTS and DISCUSSION

Isoprene synthase cDNA from *Populus alba* (PaIspS) was isolated by RT-PCR. This *PaIspS* mRNA, which was predominantly observed in the leaves, was strongly induced by heat stress and continuous light irradiation, and was substantially decreased in the dark, suggesting that isoprene emission was regulated at the transcriptional level (Fig.1). The subcellular localization of PaIspS protein with green fluorescent protein fusion was shown to be in plastids. PaIspS expressed in *E. coli* was characterized enzymatically: optimum pH of approximately 8.0, optimum temperature 40°C. Its preference for divalent cations for its activity was also studied. This optimum temperature is consistent with that the highest isoprene emission occurred between 30°C and 40°C.

Fig. 1 Expression analyses of *PaIspS* mRNA

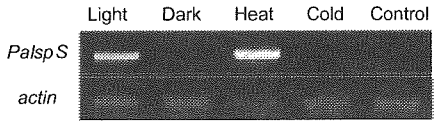

Light, continuous light (170 μmol m^{-2} s^{-1}) at 25℃ for 24 hr; Dark, continuous dark at 25℃ for 24 hr; Heat, continuous light (120 μmol m^{-2} s^{-1}) at 40℃ for 6 hr; Cold, continuous light (120 μmol m^{-2} s^{-1}) at 15℃ for 6 hr; Control, 16 hr-light (120 μmol m^{-2} s^{-1}) / 8 hr-dark at 25℃ for 24 hr.

It has reported that temperature affects isoprene emission *in vivo*. The highest isoprene emission occurred between 30°C and 40°C. This observation is consistent with the transcriptional induction by heat stress and the optimum temperature of PaIspS determined in this study.

These results also suggest that its enzyme activity may be positively regulated under illumination in plastids because photosynthetic electron transport results in the accumulation of Mg^{2+} in the stroma, along with an increase in stromal pH. In addition to the transcriptional activation of *PaIspS* by light, this is advantageous for the production of isoprene under strong light conditions. In this study, it has indicated that the physiological function of emission of isoprene from plants is defense response against the heat and strong light stress.

REFERENCES

Sasaki, K., Ohara, K. and Yazaki, K. (2005) FEBS Lett. 579: 2514-2518

Overexpression and functional analysis of a membrane-bound aromatic prenyltransferase LePGT-1 in *Lithospermum erythrorhizon*

Koji Mito
Laboratory of Plant Gene Expression, RISH, Kyoto University

Aromatic substrate prenyltransferases widely occur from bacteria to human as a subfamily of the prenyltransferase family. They play important roles in the biosysthesis of quinones molecule, such as ubiquinone and vitamine E. One of the most intensively studied members is *p*-hydroxybenzoate : polyprenyltransferase involved in ubiquinone biosynthesis. Thus far, yeast gene *Coq2* and *Arabidopsis* gene *AtPPT1* were characterized in plants and they showed broad substrate specificity for prenyl chain length, whereas a member isolated from *Lithospermum erythrorhizon*, LePGT-1, showed strict substrate specificity for geranyl diphosphate. These members have 8 and 9 transmembrane domains, and the ubiquinone biosynthetic protein members are located at mitochondria, while LePGT-1 involved in shikonin biosynthesis in localized at ER membrane.

To understand the molecular mechanism of this unique enzymatic reaction, i,e. aromatic protein substitution with prenyl chain by C-C bound formation, we tried to establish an expression system of LePGT-1 aiming at the X-ray crystallographic analysis of this protein subfamily. In this study, we have established a heterologous expression system of LePGT-1 with baculovirus in insect cultured cells (Sf9), and a purification protocol of LePGT-1 retaining its catalytic function. With purified enzyme, kinetic parameters were determined.

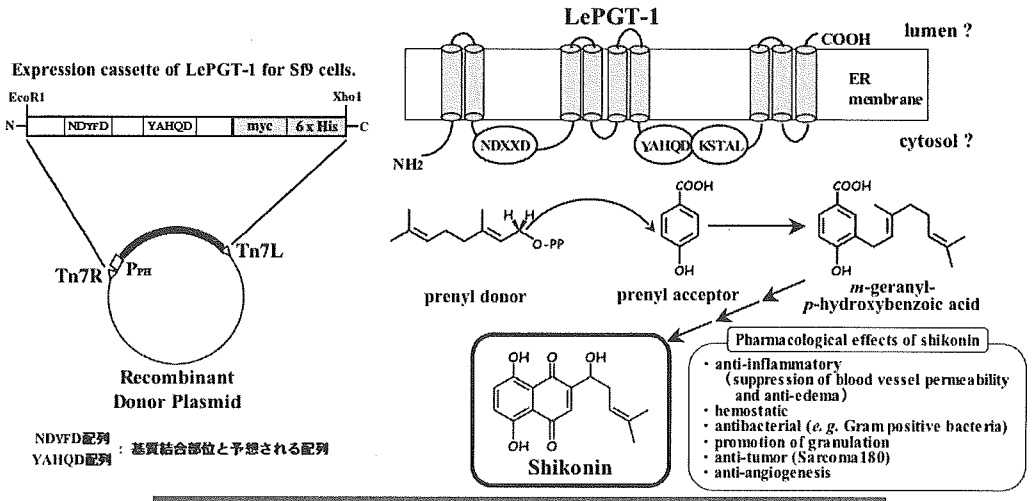

Fig. 1 Putative structure and reaction mechanism of LePGT-1

Screening of ectomycorrhizal fungi for mycorrhizal remediation of toxic heavy metals

Jilani Tahsin
Laboratory of Metabolic Science of Forest Plants and Microorganisms, RISH, Kyoto University

Heavy metal contamination caused by either natural process or human activities is one of the most serious environmental problems on earth. Phytoremediation composed of herbaceous plants and the symbiont arbuscular mycorrhizal fungi (AMF) in nature has been applied to remediate soil pollution by taking up toxic metals from the polluted soils through the roots and hyphae. However, the present author expects that a novel mycorrhizal remediation system composed of woody plants associated with ectomycorrhizal (ECM) fungi is more effective than the phytoremediation with herbaceous plants associated with AMF on the following points: 1) The mycorrhizal remediation system may remediate wider and deeper area in the soil compared to phytoremediation using herbaceous plants with AMF. 2) ECM fungi may produce greater amounts of organic acids than plant roots. The acids are essential to solublize water insoluble metal salts to give metal organic acid chelates which are expected to be taken up through mycelia and plant roots. Therefore, the objective of this study is to screen out ECM fungi for development of mycorrhizal remediation of toxic heavy metals. Several ECM fungi have been chosen as candidates for mycorrhizal remediation.

Characterization of *Asparagus officinalis* hinokiresinol synthase

Masaomi Yamamura
Research Institute for Sustainable Humanosphere, Kyoto University

Norlignans, which have a diphenylpentane (C6-C5-C6) structure, were found in coniferous trees and some monocotyledonous plants including *Asparagus officinalis* [1,2]. Their biosynthesis is of interest especially in relation to heartwood formation, a metabolic event specific to woody plants, because norlignans are deposited specifically in tree heartwood regions. This implies that the molecular mechanisms can be a clue to help us elucidate mechanisms for metabolic events specific to woody plants.

Hinokiresinol is the simplest norlignan compound, it is therefore a good target for the study of norlignan biosynthesis. Hinokiresinol has two geometrical (*E*)- and (*Z*)-isomers, which are phytoalexins of *Cryptomeria japonica* (Japanese cedar) and *A. officinalis*, respectively. Recently, biosynthetic processes and enzymatic formation of (*E*)- and (*Z*)-hinokiresinols were demonstrated using *C. japonica* and *A. officinalis* cells, respectively [2-4].

In the present study, cDNAs encoding *A. officinalis* (*Z*)-hinokiresinol synthase were cloned for the first time and their recombinant proteins were characterized biochemically.

References

[1] T. Umezawa: *Regul. Plant Growth Dev.*, 2001, 36, 57.
[2] S. Suzuki, T. Umezawa, and M. Shimada: *J. Chem. Soc. Perkin.*, 1, 2001, 3252.
[3] S. Suzuki, T. Nakatsubo, T. Umezawa, and M. Shimada: *Chem. Commun.*, 2002, 1088.
[4] S. Suzuki, M. Yamamura, T. Nakatsubo, T. Hattori, M. Shimada, and T. Umezawa: *Chem. Commun.*, 2004, 2838.

cDNA cloning and subcellular localization of glyoxylate dehydrogenase from brown-rot fungus *Fomitopsis palustris*

Madoka Fujimura
Laboratory of Metabolic Science of Forest Plants and Microorganisms, RISH, Kyoto University

Oxalate biosynthesis in wood-destroying fungi, including *Fomitopsis palustris*, has been receiving much attention, because the acid is closely associated with wood decay processes and inactivation of copper-containing wood preservatives. Wood-rotting basidiomycete *F. palustris* acquires biochemical energy for growth by oxalate biosynthesis during glucose oxidation. Two enzymes have been proposed to be involved in oxalate production for *F. palustris* by biochemical studies regarding enzyme activities. One is oxaloacetase which catalyzes hydrolysis of oxaloacetate to give oxalate and acetate. The other is glyoxylate dehydrogenase (FPGLOXDH1) to give oxalate from glyoxylate in the presence of cytochrome *c* as an electron acceptor. In this study cDNA *FPGLOXDH1* encoding FPGLOXDH1 has been cloned out and subcellular localization of FPGLOXDH1 has been investigated.

Characterization of shikonin vesicle transport mechanisms in *L. erythrorhizon* root cultures

Mariko Yano
Labolatory of Plant Gene expression, RISH, Kyoto University

Lithospermum erythrorhizon Sieb. et Zucc. (Boraginaceae) is a medicinal herb that accumulates red naphthoquinone pigments shikonin derivatives in roots. These compounds show antibacterial, wound-healing and anti-tumor activities and the dried roots are used as natural medicine. Two key precursors, *p*-hydroxybenzoic acid (PHB) derived from the phenylpropanoid pathway, and geranyl pyrophosphate synthesized through the mevalonate pathway, couple to form *m*-geranyl *p*-hydroxyl benzoic acid, and further reaction such as ring-forming and oxidation lead the formation of shikonin. It was reported that shikonin biosynthesis in *L. erythrorhizon* suspension cultures were regulated by various elements, such as Cu^{2+} ion, methyl jasmonate and oligogalacturonide which induced shikonin production, whereas ammonium ion, glutamine and light irradiation inhibited shikonin formation. In particular, light is the strongest inhibitor of shikonin biosynthesis.

Shikonin is secreted out of the cell presumably via vesicle transport pathway from ER to plasma membrane. In *L. erythrorhizon* pigment-producing cells, a large number of spherical bodies (0.1-0.2 um) or swellings which were filled with substance of high electron density were specifically found in ER by electron microscopic observation. To investigate shikonin transport by a molecular biological approach, genetic viewpoint, we applied PCR-select subtraction to *L. erythrorhizon* cells cultured in dark (shikonin producing) or light irradiation (non-producing) to isolate genes involved in shikonin production systematically.

In the PCR-select subtraction, we picked up 242 clones that were induced in the dark, whereas only 7 clones were obtained as UP-regulated genes under illumination, which were more than 5 times down or up regulated out of 1152 clones investigated. The high preference for dark-inducible genes was a characteristic for *L. erythrorhizon* cultured cells that synthesize the lipophilic secondary metabolite specifically in root. The BLAST search revealed that 70% of dark-inducible 242 genes were coding for metabolic enzymes, in which known shikonin biosynthetic enzymes like Le-PGT (*L. erythrorhizon* PHB Geranyltransferase) and HMG-CoA reductase. Beside these biosynthetic genes, 3% were transporters, 4% were receptors, transport signals, and transcription factors, as well as 23% of genes of unknown. However no genes related to vesicle transport were found in the list, suggesting that capable of transporting shikonin were not regulated by light at reast at the transcriptional level.

To thoroughly analyze genes involved in shikonin production, we carried out EST analysis of *L.erythrorhizon* cells in shikonin-producing condition. BLAST analysis with 10,000 clones revealed that adding to some known shikonin biosynthetic enzymes like Le-PGT or HMGCoA reductase, many genes relevant to vesicle transport were obtained. They are classified into several groups, i.e., COP II components which carry transport vesicles from ER to Golgi anterograde pathway, COP I components which transport vesicles from Golgi to ER retrograde pathway, clathrin heavy and light chains which play important role in various route of vesicle transport, and clathrin adopter proteins.

As shikonin derivatives are very hydrophobic compounds, they are presumed to be compartmented in lipid monolayer vesicles. All known vesicle transport mechanisms so far are elucidated for lipid bilayer vesicles, and lipid monolayer vesicle transports is yet unidentified. However, these maybe some common protein members which COP I, COP II, and clathrin-mediated vesicles taking part in the intercellular transport of lipid monolayer vesicles in *L. erythrorhizon*. I expect that EST information obtained in this study will contribute to clarify the shikonin vesicle transport mechanism at molecular revel.

Study on Wireless Power Distribution System for Buildings

Tatsuhiko Adachi

Laboratory of Space Radio Science, RISH, Kyoto University

INTRODUCTION

Building designs that aims at the convenient improvement of the floor outlet and the free access floor have recently increased. However, the construction cost is expensive. Moreover, in architectural industry, the structure that can flexibly correspond to the demand that diversifies and upgrades along with an economic activity are hoped for. In this research, we suggest wireless power distribution system for buildings as a new application of microwave power transmission in order to solve the above-mentioned problem. This system supplies electric power wirelessly by using building materials as a microwave transmission line. The purpose of the present research is to confirm the feasibility and to clarify the technical problems.

DECK PLATE WAVEGUIDE

First, we described analyses and experimental results concerning basic characteristic of the deck plate waveguide. As a result, we have found out the connection method between the deck plate and the cover board is important to transmit microwave power efficiently. The attenuation constant of the deck plate waveguide was measured to be 0.02dB/m when the contact resistance between the deck plate and the cover board was reduced.

MICROWAVE POWER DISTRIBUTION SYSTEM

We developed the variable power divider whose changeability is from -10dB to -3dB. And we constructed the power distribution system that actively did the distribution control. Next, we examined the methods to take out microwave power from the deck plate waveguide. And, we analyzed the method of using a coaxial probe and established the design technique.

SUMMARY

Finally, we did a practical examination of the whole system based on the abovementioned experiments. As a result, total efficiency is 45%. And we designed the wireless power distribution system in detail, and explained its technical problems.

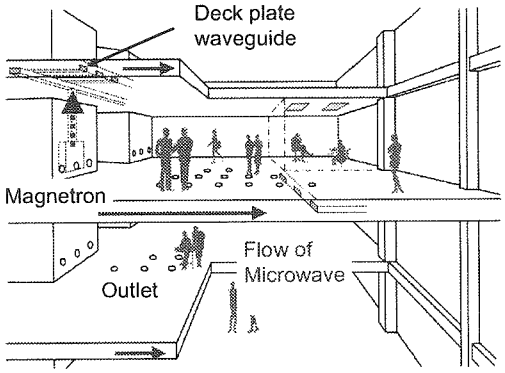

Figure 1 Conceptual diagram

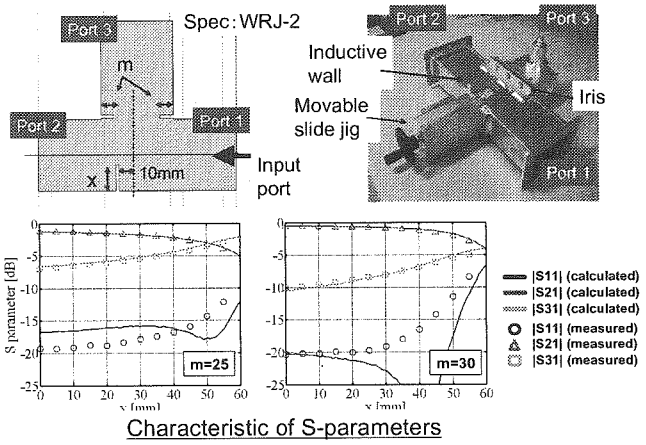

Figure 2 Variable Power Divider

Computer experiments on the characteristics of electric field antenna in the spacecraft environment

Yohei Miyake
Laboratory of Space Radio Science, RISH, Kyoto University

The characteristics of electric field antennas installed on board the scientific satellites are studied by making use of the Particle-In-Cell (PIC) plasma simulations. The precise calibration of plasma wave data obtained by spacecraft observation requires the knowledge of antenna impedance in the space plasma environment. However, the plasma environment near the spacecraft, which becomes non-uniform due to the plasma kinetic effects such as sheath formation and photoelectron emission, is so complex that it is difficult to be treated by theoretical approaches.

To treat the antenna model including a spacecraft body and analyze the effects of photoelectron emission on antenna characteristics, we applied the PIC simulation method to the conventional FDTD method in the present study. Figure 1 shows the model of the present computer experiment. The present antenna model, which is immersed in background plasma, consists of perfect conducting antennas and spacecraft body. We also modeled the photoelectron emission from the sunlit surfaces of conducting body with an assumption of the arrival direction of sunlight.

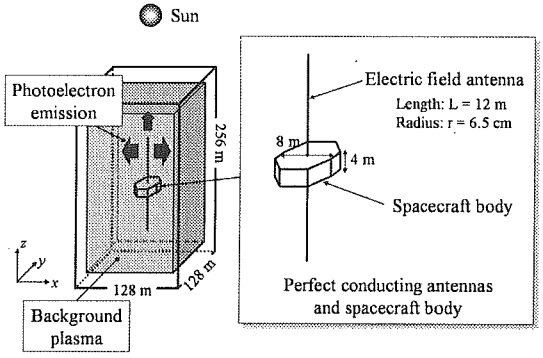

Figure 1: Simulation model.

Using these models, we first conducted the electrostatic simulations focused on photoelectron sheath formation around the spacecraft. The obtained electron density profile (Figure 2) shows that the electron dense region caused by photoelectrons is created around the sunlit antenna and spacecraft surface. Meanwhile, the sunless antenna is negatively charged with impinging background electrons and made the electron sparse region. It was also confirmed that the plasma environment depended sensitively on the incident angle of sunlight which determined the location and amount of photoemission.

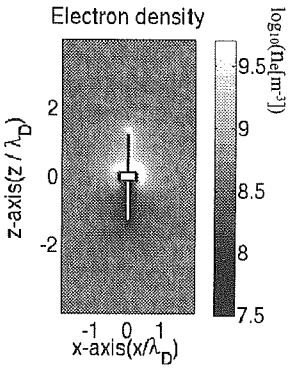

Figure 2. Contour map of electron density.

Next, the antenna impedance under the obtained plasma environment was examined by the electromagnetic simulations. Figure 3 shows the obtained results of imaginary part of impedance. Obtained results for both resistance and reactance were much different from those in vacuum below the characteristic frequency corresponding to the local density in photoelectron sheath. The difference of impedance characteristics between sunlit and sunless antennas was also found. This suggests that the impedance characteristics vary with the spin or attitude change of spacecraft. Now we start to consider the real plasma parameters of the Earth's magnetosphere and examine the antenna impedance. These analyses will contribute to the calibration of plasma wave data obtained by spacecraft observations and the design of electric field antennas aboard the future mission.

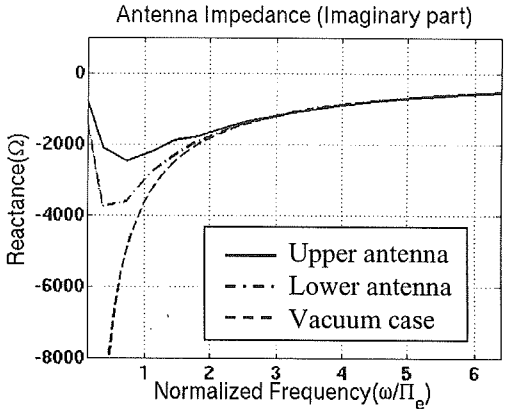

Figure 3: Imaginary part of impedance (reactance).

REFERENCES

[1] H. Usui, Y. Miyake, M. Okada, Y. Omura, and the GES project team, Development and Application of Geospace Environment Simulator for the Analysis of Spacecraft-Plasma Interactions, Submitted to IEEE Plasma Science, 2005.

Study on Pulse-driven Phase Controlled Magnetron

Takaaki Matsushima
Graduate School of Engineering, Kyoto University

The object of the present study is to develop a pulse-driven PCM(Phase Controlled Magnetron). A PCM has been originally developed for a microwave source of a microwave power transmission system. The pulse-driven PCM for radar systems has a possibility for an additional application. Also, a key feature of the pulse-driven PCM is adjustment of the output microwave power by pulse width control. Compared to semiconductor devices, a PCM is efficient, inexpensive and light. However the previous PCMs are driven in CW mode and they need three second to control the phase. Therefore, the response time of the PCMs is necessary to be improved to develop a pulse-driven PCM and high-speed beam directional control for a microwave power transmission system.

The PCM developed by our study group can stabilize its phase and its oscillating frequency by combination of the injection locking method and controlling anode current of the magnetron with a PLL(Phase-Locked Loop) technique.

First, we experimentally succeeded in a high-power microwave beam forming with SPORTS2.45 (Space POwer Radio Transmission System for 2.45GHz). We also analyzed the effect of phase fluctuation on microwave beam pattern.

Next, we optimized a PLL system of the previous PCM. Response time of the optimized PCM is about 1.6ms. Furthermore, we designed a new phase control system for a high voltage power supply with quick response time and succeeded in speed-up of the phase control system. As the result, the response time is improved to be about 0.2ms.

Finally, we developed a kHz-class pulse-driven PCM by the improved PCM. The pulse-driven PCM was able to stabilize its phase within 0.1ms in most pulses. Furthermore, we suggested a MHz-class PCM control system, which is designed with a standard weather radar system.

Development of a wireless charging system for an electric vehicle

Kenji Shinoda
Graduate School of Engineering, Kyoto University

In this thesis, we study on development of a wireless charging system for an electric vehicle (EV) with wireless microwave power transmission (WPT) at 2.45GHz. Generally the EV may contribute to energy problems and environment affairs because of two features. One is that the EV is superior to a gasoline motorcar in the total energy conversion efficiency from fossil fuels. Another is that the EV has few exhaust gases. However, the EV has defects such as low mile and slow charging. To defeat these disadvantages, we developed a wireless rapid charging system with WPT.

Firstly, we explained configuration and components of the wireless charging system. In this system, the components have to be designed with high microwave density. Hence, we newly developed high power rectennas of 13W with RF-DC conversion efficiency of 52%.

Secondly, we experimented on the whole wireless charging system to the EV. The experiment was conducted with 5 transmitting systems and 81 receiving systems. As the experimental result, we succeeded the energy charging of 333kJ in 70 minutes with WPT.

Thirdly, we investigated the dependence of a distance between the transmitting antennas and the receiving antennas to establish an efficient wireless charging system. From this investigation, accordingly we found out that charging power has the distance regularity of an approximate$\lambda/4$periodicity.

Finally, we researched the relation between RF-DC conversion efficiency and diode SPICE parameters, and represented that SiC devices is the best match to a rectenna's diode by own performance in the future.

Study of electromagnetic coupling of midlatitude ionosphere *E* and *F* regions with VHF radars and GPS-TEC observations

Akinori Maegawa
Laboratory of Radar Atmosphere Science, RISH, Kyoto University

Various types of plasma instabilities have been studied in the mid-latitude ionosphere *E*- and *F*-region. FAIs (Field Aligned Irregularities) in both regions is one of them. The *E*-region FAIs (*E*-FAIs) are assumed to be caused by the polarization electric field in the electronic density perturbation of the *Es* layer. The *F*-region FAIs (*F*-FAIs) are thought to be generated by the polarization electric field at the wall of the TIDs (Traveling Ionosphere Disturbances). In the ionosphere, conductance parallel to the geomagnetic filed is so high that such polarization electric fields are easily mapped along the field line for several hundred kilometers. Because of these characteristics, electromagnetic coupling is expected between the *E*- and the *F*-region. In this research, we discussed such *E*-*F* coupling process from the results of FERIX (*F*- and *E*-Region Ionosphere Coupling Study) campaign in 2004 and statistical comparison of radar observation of *E*-FAIs and the GPS-TEC perturbation over Shigaraki in 2005.

During the FERIX campaign, using the MU radar for *F*-FAIs observation and LTPR (Lower Thermosphere Profiler Radar) for *E*-FAIs observation, we succeeded to observe the coupling of *E*-FAIs and *F*-FAIs that occurred simultaneously along the same magnetic field lines. We also found that the horizontal structures of *E*-FAIs, *F*-FAIs and TIDs are all aligned from northwest to southeast, and propagated to the west at the same speed. Fig1 is a significant example of such result. Fig1(a) shows the comparison of *E*-FAIs (color dot) and *F*-FAIs (gray contour). The spatial structures of *E*-FAIs were determined by the LTPR interferometry and those of *F*-FAIs were determined by the 16 beams observation technique of the MU radar. The coordinates of *F*-FAIs were arranged from altitude 300km to 100km along the field line in order to compare with *E*-FAIs. Fig1(b) shows the comparison of *F*-FAIs and perturbation TEC (color contour), both of which were arranged to altitude 300 km. At that time, we can see all structures are aligned NW to SE.

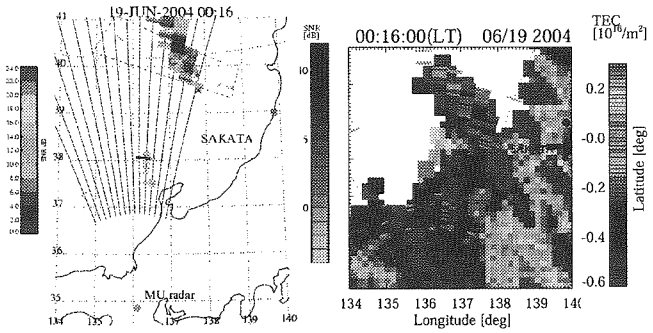

(a) (b)

Fig1

During the continuous observation in 2005, data from the experiment were compared with GPS-TEC data from the GEONET for statistical study for the *E*- and *F*-region coupling processes. At first, we determined the position where the *E*-FAIs echoes were often observed with LTPR, and mapped them to the *F*-region (300 km altitude) along the field line. Perturbation of the GPS-TEC (pTEC) at that point was compared with *E*-FAIs activity determined from the LTPR echo power. Within 64 samples, in 34 cases, there were clear correlations between the *E*-FAIs occurrence and large fluctuation of pTEC. Fig2 is a typical example of clear correlation. We investigated the *F*-region plasma structure such as azimuth-dependent structure of MSTIDs (Medium-Scale Traveling Ionospheric Disturbance) of such case. The result showed that the angle distribution of pTEC horizontal structure for the case had a prominent angle distribution of about -50 to –20 (Fig3). We discussed that this shows developed MSTIDs exist when *E*- and *F*-region coupling occurred.

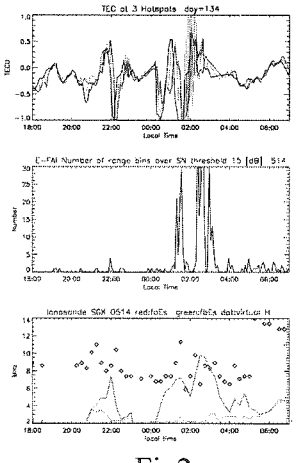

Fig2

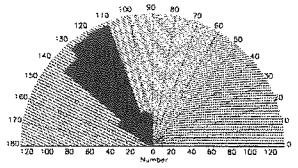

Fig3

From these results, we found several direct evidences of electromagnetic coupling between the *E*- and the *F*-regions. When the coupling is observed, northwest-southeast aligned structures were often seen in both regions. This is consistent with the theoretical study by Cosgrove et al., 2004.

Observation of Refractive Index Profiles with GPS Radio Occultation from an Airplane

Satoshi Danno
Laboratory of Atmospheric Sensing and Diagnosis, RISH, Kyoto University

INTRODUCTION

In recent decades, climate changes, such as global warming and El Nino, have significantly influenced the stable living environment and sustainable development of human society. Floods, severe rains and huge typhoons connected to climate change have caused a great deal of destruction. In order to improve. the forecasting of severe weather, such as heavy rain, accurate observations of water vapor (WV) distributions having large time and spatial variations should be incorporated into the numerical weather prediction (NWP) model (data assimilation). The Global Positioning System (GPS) radio occultation (RO) technique is a useful application of the precise satellite positioning system for monitoring the Earth's atmosphere (GPS meteorology).

METHODS AND EXPERIMENTS

The GPS RO technique is based on measurement of the bending and delay of GPS radio waves when passing through the atmosphere (Fig. 1). The bending and delay in the neutral atmosphere are converted to a refractive index profile for each occultation event. Since the refractivity is the function of atmospheric temperature and WV mixing ratio, GPS RO data can provide a detailed WV profile with a high vertical resolution. This observation may be done in the space with a GPS receiver on low-earth-orbit satellites or within the atmosphere by situating a receiver on mountaintop or airplane. In the present study, the GPS RO technique for a receiver located in an airplane was developed for the first time. The technique was applied to field experiments using a GPS receiver newly developed for airborne GPS occultation measurements onboard an aircraft of the Electronic Navigation Research Institute (Fig. 2).

RESULTS AND CONCLUSIONS

For the GPS RO observation from the airplane, the following were developed: (1) a new GPS receiver system that has a high sensitivity capable of detecting a weak GPS RO signal at a high sampling rate, (2) an accurate positioning system by combining the GPS and an Inertial Measurement Unit (IMU) in order to determine the airplane velocity with an accuracy of up to 5 mm/sec, and (3) the retrieval software for the refractive index profile, in particular, a technique by which to derive the bending angle around zero elevation angle. More than 70 occultation events were obtained from nine airborne GPS RO campaign experiments conducted from Oct. 2003 to Feb. 2005. Analyzing the experimental data by the software developed herein, the refractive index profiles, which were consistent with the balloon-based observations (radiosonde) and NWP model, were retrieved. An example is shown in Fig.3. The application of this technique to all available commercial airplanes in the future is expected to enable a tremendous amount of WV information to be routinely obtained.

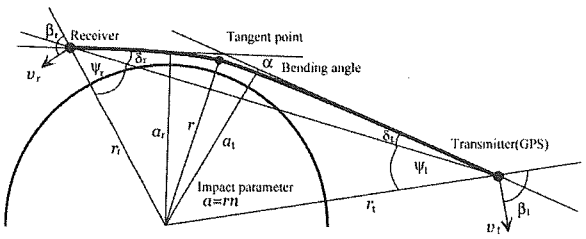

Figure 1 Schematic illustration of the GPS RO

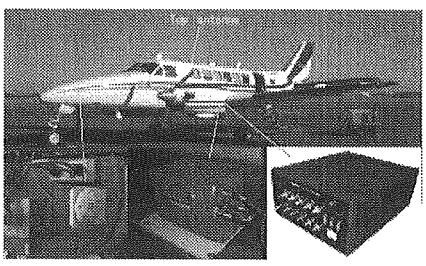

Figure 2 The aircraft and the receiver system.

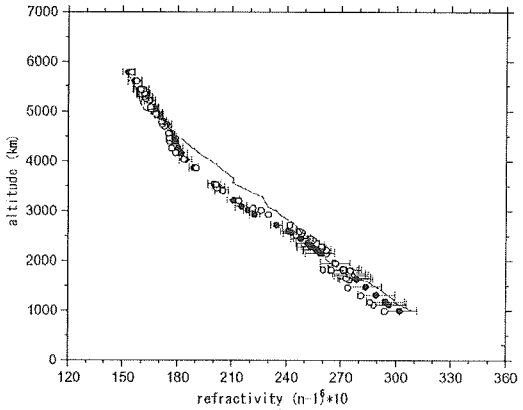

Figure 3 Example of the derived refractivity profiles. Solid: Derived from GPS RO. Circles: reference data for comparison (numerical weather prediction data)

Development of A New Humidity-Retrieval Algorithm from Turbulence Echo

Shingo Imura
Laboratory of Atmospheric Sensing and Diagnosis, RISH, Kyoto University

INTRODUCTION

The behavior of the atmosphere is characterized by various physical parameters. Humidity is one of the most important driving forces of intense atmospheric disturbance via the latent release of heat. Although the amount of water vapor generally decreases with increasing height, it shows large variations in time and space, e.g., with the passage of a front or clouds. It is very important to develop a new and accurate technique for continuously monitoring the humidity profile, regardless of weather conditions. Humidity profiles obtained via advanced measurement methods are useful for studying meteorological phenomena, global environmental change, and disaster prevention.

The turbulence echo intensity observed by wind-profiling radar is closely related to the vertical gradient of refractive index squared (M^2), which largely depends on the vertical humidity gradient in the moist atmosphere. In previous studies, height profiles of humidity have been estimated from these characteristics by determining the sign of the radar-derived $|M|$ using simultaneous complementary measurements. Wind-profiling radar has great potential as a tool for all-weather humidity observations. To put this device into practical use, however, it is first necessary to improve the accuracy and expand the height range.

HUMIDITY RETRIEVAL WITH THE MU RADAR AND LOWER TROPOSPHERE RADAR

The height range of humidity retrieval was expanded by combining data from MU (middle and upper atmosphere) radar with RASS (Radio Acoustic Sounding System) and Lower Troposphere Radar (LTR) operating at 46.5 MHz and 1.3 GHz frequencies, respectively. Reduction of the MU radar receiver sensitivity was undertaken to prevent the leakage of transmission signal to the receiver; this was corrected by comparing the signal-to-noise ratio (SNR) of the MU radar and LTR below 2.1 km height. $|M|$ profiles from the two radars between 1.5 km and 1.95 km height are then merged with a linear weighting function. Specific humidity (q) profiles were successfully estimated from the merged $|M|$ profiles.

HUMIDITY RETRIEVAL USING A ONE-DIMENSIONAL VARIATIONAL METHOD

To achieve a more precise estimate of humidity, a one-dimensional variational method was applied using a wind-profiling radar. A statistical probability for the sign of M is introduced to the cost function of the variational method to determine the optimum result with reduced calculation cost. Humidity profiles were retrieved from the MU radar-RASS data using the first guess calculated from the time-interpolation of radiosonde results. Figure 1 shows time-height variations in the radiosonde-derived q (upper), the first guess (middle) and the analysis result (lower). The time-height structure of the radiosonde-derived q shows remarkable features that are highlighted on the figure by circles. The radiosonde result has a sharp peak below 3.9 km height at 18:00 LT on July 31 and two peaks at 3.0 km height at 09:00 LT and 15:00 LT on August 1. It is also apparent that the radiosonde result below 3.0 km decreased over time between 12:00 LT and 21:00 LT on August 3; however, these structures are not evident in the time-height variation of the first guess calculated from the time-interpolation of 12-hourly radiosonde results. Time-height variations in the analysis result are in good agreement with the recorded variation in the radiosonde result, especially the remarkable peak as shown by circles. This result confirms that the analysis result successfully retrieved detailed humidity variations that cannot be expressed by the first guess. The remarkable improvement over the conventional method is especially evident for the case of a large error in the first guess.

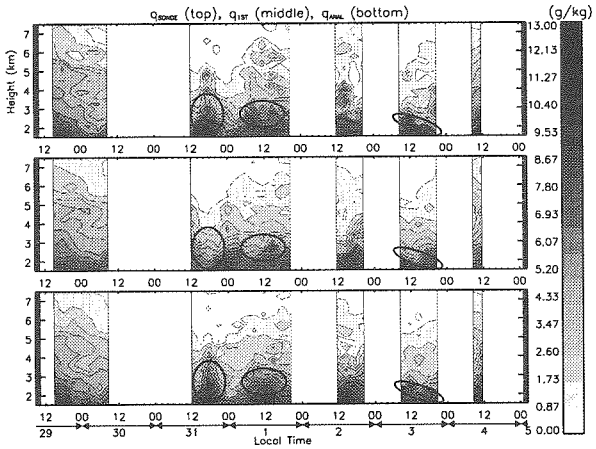

Figure 1 Time-height variation in the radiosonde-derived q (upper), the first guess (middle) and the analysis result (lower). Note that the first guess profiles are calculated from 12-hourly radiosonde results.

Development of a water vapor Raman LIDAR for boundary layer observation

Naohiro Sugimoto
Laboratory of atmospheric sensing and diagnosis, RISH, Kyoto University

We have developed a portable Raman lidar system for profiling water vapor which is one of the most important atmospheric properties in the tropospheric weather system. Water vapor Raman lidars usually use a large power laser and the mobility is limited. However, our new lidar system is a compact and transportable system by using small Nd:YAG laser (SHG:532 nm, 30 mJ, 20 Hz) by focusing on boundary layer measurements up to 3 km. The received lights collected with a 35.5 cm telescope are measured by photon counting system for elastic (532 nm), N_2 Raman (607 nm) and H20 Raman (660 nm) signals, respectively. The weight of the major component of the system is about 75 kg with a dimension of 50 cm x 50 cm x 150 cm, and the system is transportable with a two person by means of a vehicle.

In the night time profiling observation, we estimated the error in humidity is smaller than 20 % up to 2 km height by 45 minutes and 200 m integration. This precision is enough for unattended humidity profiling planned for the humidity observations in the Asia monsoon region.

Horizontal distribution of waver vapor was observed for the night time, at Shigaraki MU observatory over the national forest. Between the distance of 400 m and 3500 m, humidity variations of an amplitude of 10 % with a horizontal scale of about 200 m were detected, correlated with variations of aerosol backscatter ratio. This suggests possibility of studying horizontal distribution of minor constituents over the forest.

We observed the volcanic gas at Mt. Aso by installing the lidar in a vehicle. Water vapor mixing ratio in the gas was 0.4 g/kg larger than that of background atmosphere (4.5 g/kg). This observation showed both the possibility of application to the volcanic study and the mobility of the developed lidar system.

To summarize, we have successfully developed a portable waver vapor Raman lidar system useful for various research regions such as meteorological, forest, and volcanic studies.

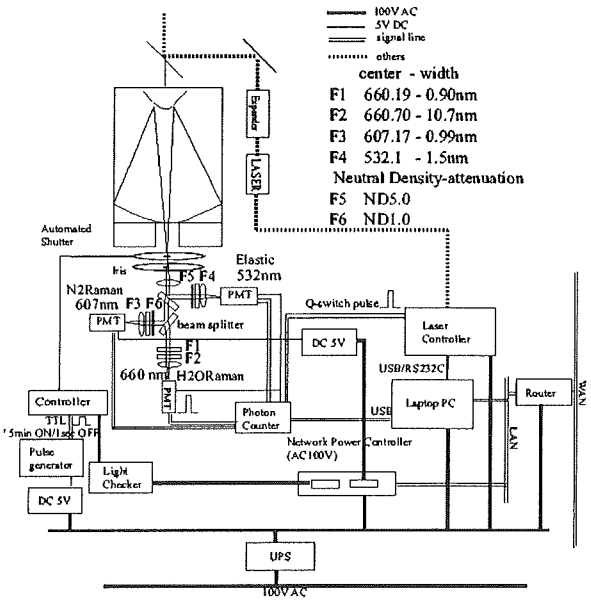

Figure 1. The block diagram of the Raman lidar system.

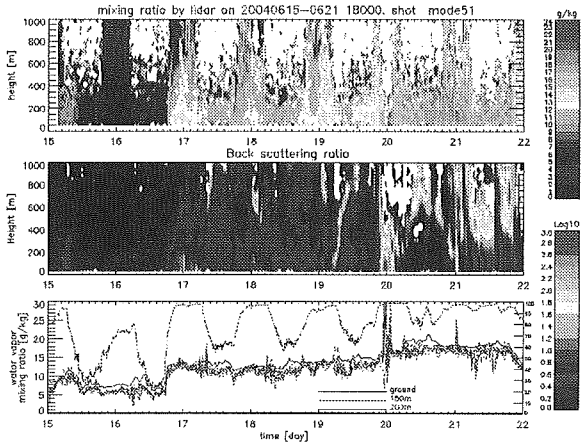

Figure 2. Time-height variations of (top) water vapor, (middle) backscatter ratio (aerosol) and water vapor mixing ratio at 200 m, 150 m, ground level with relative humidity (bottom).

ABSTRACT (MASTER THESIS FOR GRADUATE SCHOOL OF SCIENCE)

Study on structural variations of Typhoon based on wind profiler observations

Hiroshi Fujita

Laboratory of Radar Atmospheric Science Division of Diagnostics and Control of Humanosphere, RISH, Kyoto University

It is known that some tropical cyclones (TCs) appeared in low latitudes transform into extratropical cyclone at mid-latitude. This process is called extratropical transition (ET), and various disasters often happen in this process. However, ET is poorly understood yet while mature TCs are rather well researched.

In this study, we mainly examined the transition processes of the wind behavior of two TCs (Typhoons 0310 and 0416) using observation data with Wind Profiler Network and Data Acquisition System (WINDAS) of Japan Meteorological Agency (JMA). When we analyze WINDAS data, transition processes of the TCs were classified into four stages based on structural variations of precipitating clouds obtained by JMA weather radars, which is familiar to the general public.In addition to the variations of wind behavior in the vicinity of TC center, variations of thermal structures and synoptic scale features were also analyzed using radiosonde and RANAL data, respectively.

Synoptic trough and ridge axis shifted eastward as TCs moved. Strong positive vorticity in the vicinity of the center, which existed in former stages, disappeared at the middle troposphere in the latter stages. Distributions of divergence and convergence at lower and upper levels also rapidly changed in the latter stages. Though dry air intruded from upper level to lower level in latter stages, we showed that transitions of precipitating clouds heavily depended on the atmospheric stratifications. Transitions of strong cyclonic winds in the vicinity of the TCs in front side well corresponded to the variations of precipitating clouds, that is, the strongest peak of cyclonic wind gradually weakened and its location shifted outward and higher altitudes. We suggested that disappearance of the strong peak of cyclonic wind could be a criterion whether TCs transformed into extratropical cyclones or not.

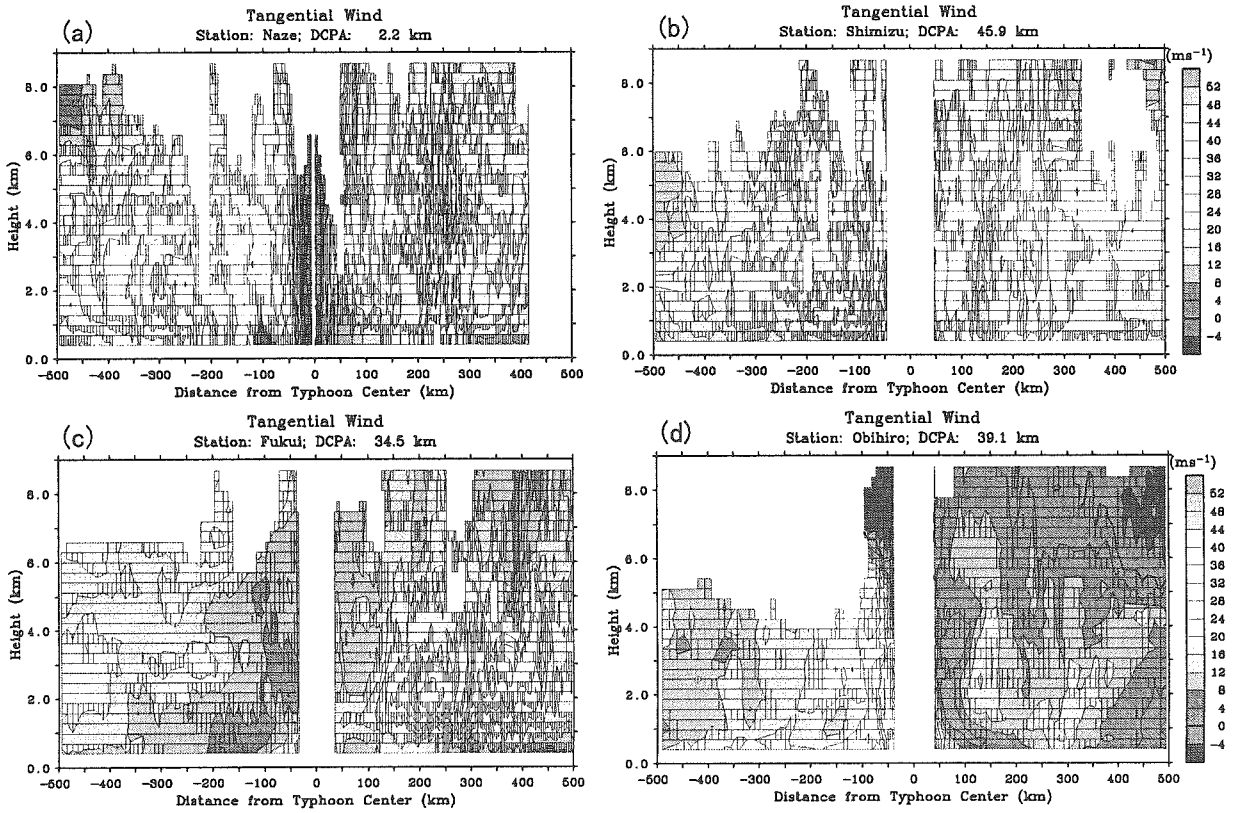

Fig. Radius-height cross sections of tangential winds relative to TC center observed by wind profilers at (a) Naze, (b) Shimizu, (c) Fukui and (d) Obihiro. The positive and negative values of radius correspond to the period when the TC approaches (in front side of TC) and leaves (in rear side of TC) to the observation sites, respectively. Positive and negative values of contour represent cyclonic and anticyclonic winds, respectively.